AD-A127 078 FIELD-OF-VIEW REQUIREMENTS FOR APPROACH AND LANDING OF 1/1
V/STOL (VERTICAL/S..(U) SYSTEMS TECHNOLOGY INC
HAWTHORNE CA W F CLEMENT ET AL. AUG 78 STI-TR-1115-1
UNCLASSIFIED NADC-77240-07 N62269-77-C-0509 F/G 1/3. NL

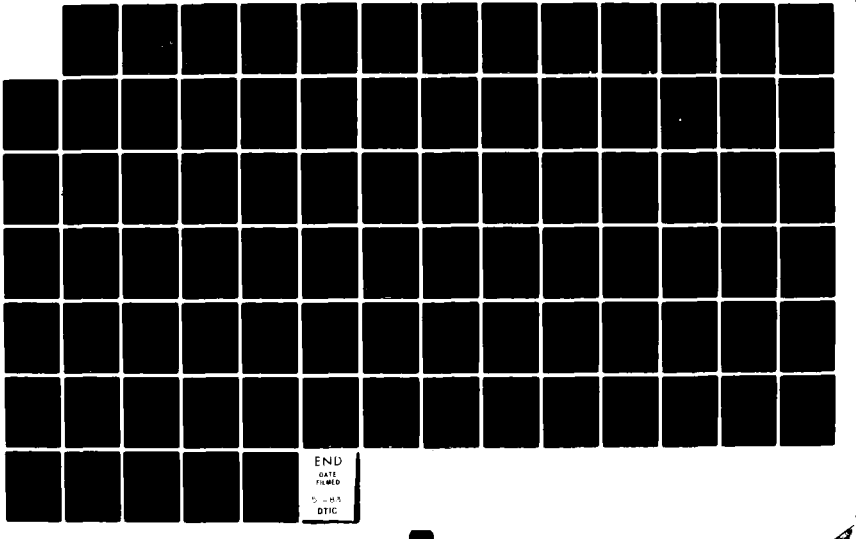

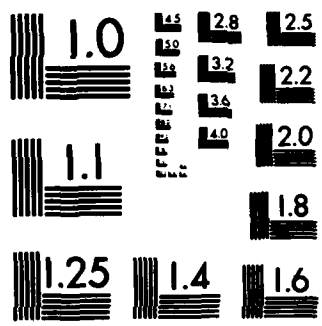

Unclassified

SECURITY CLASSIFICATION OF THIS PAGE (When Data Entered)

REPORT DOCUMENTATION PAGE

READ INSTRUCTIONS BEFORE COMPLETING FORM

1. REPORT NUMBER: NADC 77240-07	2. GOVT ACCESSION NO.: AD-A127078
3. RECIPIENT'S CATALOG NUMBER:	
4. TITLE (and Subtitle): FIELD OF VIEW REQUIREMENTS FOR APPROACH AND LANDING OF VSTOL AIRCRAFT	5. TYPE OF REPORT & PERIOD COVERED: Final - 1 October 77 - 31 August 1978
	6. PERFORMING ORG. REPORT NUMBER: STI TR 1115-1
7. AUTHOR(s): Warren F. Clement, Robert K. Heffley, Wayne F. Jewell	8. CONTRACT OR GRANT NUMBER(s): N62269-77-C-0509
9. PERFORMING ORGANIZATION NAME AND ADDRESS: Systems Technology, Inc. 13766 South Hawthorne Boulevard Hawthorne, Ca. 90250	10. PROGRAM ELEMENT, PROJECT, TASK AREA & WORK UNIT NUMBERS: 63257N - V/STOL W0589 RD603
11. CONTROLLING OFFICE NAME AND ADDRESS: Naval Air Systems Command Department of the Navy Washington, D.C. 20361	12. REPORT DATE: August 1978
	13. NUMBER OF PAGES: xii + 71
14. MONITORING AGENCY NAME & ADDRESS (if different from Controlling Office): Naval Air Development Center VSTOL Program Office Warminster, Pa. 18974	15. SECURITY CLASS. (of this report): Unclassified
	15a. DECLASSIFICATION/DOWNGRADING SCHEDULE

16. DISTRIBUTION STATEMENT (of this Report)

Distribution unlimited

17. DISTRIBUTION STATEMENT (of the abstract entered in Block 20, if different from Report)

18. SUPPLEMENTARY NOTES

19. KEY WORDS (Continue on reverse side if necessary and identify by block number)

VSTOL (Vertical/Short Take-off and Landing)
Visual Requirements
Pilot Modeling

20. ABSTRACT (Continue on reverse side if necessary and identify by block number)

A rationale for quantifying fixed wing V/STOL aircraft field of view requirements is developed and illustrated by a variety of examples involving shipboard recovery. The analytic technique employed involves the dynamic modeling of (a) the recovery guidance and control situation, (b) the disturbance environment, (c) the augmented aircraft, (d) the pilot's multiloop control activities, (e) the perceptual behavior of the pilot as affected by the limitations associated with visibility and divided attention, and

DD FORM 1 JAN 73 1473 EDITION OF 1 NOV 65 IS OBSOLETE

Unclassified

SECURITY CLASSIFICATION OF THIS PAGE (When Data Entered)

(f) the resulting geometric properties of informative elements within the visual field. The foregoing factors are combined to enable the analyst to identify those areas of the field of view which are essential for perception of the cues necessary for guiding and controlling the powered-lift aircraft to a safe recovery. The analytic technique accounts for the combined variability in field of view caused by rolling, pitching, yawing, surging, swaying and heaving degrees of freedom of the aircraft as the pilot attempts to guide and control the aircraft over the recovery area on the moving ship. The required field of view is a function of (1) the location of the pilot's point of regard on the ship, (2) the aircraft orientation, and (3) the relative position of the aircraft with respect to the ship, but in practice the field of view may be restricted by cockpit occlusions. The resulting field of view requirements depend in a critical way on the predicted model of the ship's airwake disturbance environment . Validation of the airwake environment for V/STOL operations with non-aviation ships, therefore, is an imperative recommendation resulting from this study.

NADC 77240-07

SYSTEMS TECHNOLOGY, INC.

2672 BAYSHORE FRONTAGE ROAD • MOUNTAIN VIEW, CALIFORNIA 94043 • PHONE (415) 961-4674

Technical Report No. 1115-1

Final Report

FIELD-OF-VIEW REQUIREMENTS FOR APPROACH AND LANDING OF V/STOL AIRCRAFT

1 October 1977 - 31 August 1978

Contract N62269-77-C-0509

Warren F. Clement
Robert K. Heffley
Wayne F. Jewell

August 1978

Naval Air Development Center
Warminster, Pennsylvania 18974

ABSTRACT

A rationale for quantifying fixed wing V/STOL aircraft field-of-view requirements is developed and illustrated by a variety of examples involving shipboard recovery. The analytic technique employed involves the dynamic modeling of (a) the recovery guidance and control situation, (b) the disturbance environment, (c) the augmented aircraft, (d) the pilot's multiloop control activities, (e) the perceptual behavior of the pilot as affected by the limitations associated with visibility and divided attention, and (f) the resulting geometric properties of informative elements within the visual field. The foregoing factors are combined to enable the analyst to identify those areas of the field of view which are essential for perception of the cues necessary for guiding and controlling the powered-lift aircraft to a safe recovery. The analytic technique accounts for the combined variability in field of view caused by rolling, pitching, yawing, surging, swaying and heaving degrees of freedom of the aircraft as the pilot attempts to guide and to control the aircraft over the recovery area on the moving ship. The required field of view is a function of (1) the location of the pilot's point of regard on the ship, (2) the aircraft orientation, and (3) the relative position of the aircraft with respect to the ship, but in practice the field of view may be restricted by cockpit occlusions. The resulting field of view requirements depend in a critical way on the predicted model of the ship's airwake disturbance environment. Validation of the airwake environment for V/STOL operations with non-aviation ships, therefore, is an imperative recommendation resulting from this study.

ACKNOWLEDGEMENTS

The authors gratefully acknowledge the sponsorship which made possible this application of a systematic theory for manual control of aircraft based on the pilot's perception of cues in the external visual field. This work was sponsored by the Naval Air Development Center, Warminster, Pennsylvania, under Contract No. N62269-77-C-0509 as part of the powered-lift flight technology program of the Naval Air Systems Command, Department of the Navy. For his guidance, encouragement and constructive criticism, we are particularly grateful to the Contract Technical Monitor, Mr. Paul M. Linton.

The authors wish also to acknowledge the sustaining technical direction provided by Mr. Duane T. McRuer, the helpful suggestions of their colleagues, and their appreciation for the painstaking effort of the Systems Technology, Inc. staff in the production of this report.

TABLE OF CONTENTS

TABLE OF CONTENTS (Concluded)

LIST OF TABLES

LIST OF FIGURES

LIST OF FIGURES (Concluded)

LIST OF ABBREVIATIONS

cm	Centimeter (unit for picture plane coordinates)
co	Complement
cos	Cosine
cot	Cotangent
csc	Cosecant
DD963 et seq	Spruance class destroyer
deg	Degree
exp	Naperian base 2.71828...
FOV	Field of View (vide SYMBOLS)
ft	Feet
GSI	Glide slope indicator
HP	Hewlett Packard
IFR	Instrument Flight Rules
kt	Knot
LOS	Line of Sight (vide SYMBOLS)
O-axis	Optical Axis (vide SYMBOLS)
PPI	Plan Position Indicator
sec	Secant
sin	Sine
tan	Tangent
VFR	Visual Flight Rules
VIA	Visual Landing Aids
V/STOL	Vertical/short takeoff and landing
WP	Working Paper

LIST OF SYMBOLS

a	Distance along O-axis between eye and picture plane; also one-half of the hangar face width or height in Table 2.
a_x	Longitudinal or horizontal acceleration, depending on the definition of the x-axis.
A	Gilinsky's effective size parameter for the point of regard in the visual field.
B	Sub- or superscript denoting aircraft-centered reference frame, aligned either with a body reference or with total velocity.
C_o	Inherent source or target luminance contrast.
C_R	Observed luminance contrast
E	Sub- or superscript denoting aircraft-centered reference frame, aligned with earth frame of reference.
E	Angle defining direction of line-of-sight from aircraft to ship with respect to total velocity of aircraft, sometimes with subscript h or v denoting horizontal or vertical plane.
FOV_λ	Lateral coordinate of a point of regard in the field of view defined with respect to the point where the aircraft logitudinal body reference axis intercepts the picture plane.
FOV_μ	Normal (orthogonal) coordinate of a point of regard in the field of view defined with respect to the point where the aircraft longitudinal body reference axis intercepts the picture plane.
g	Gravitational acceleration
h	Altitude
i	Index identifying point of regard in the visual field; also used as a subscript; $i = 1,2,\ldots$.
K	Controlled element response proportionality factor.
K_n	Visual guidance proportionality factor for motion normal to trajectory.
K_t	Visual guidance proportionality factor for motion tangential to trajectory.

SYMBOLS (continued)

ℓ	Arc length of one plane square segment of the partitional spherical visual field.
LOS_h	Relative bearing of line of sight along O-axis with respect to ship centerline.
LOS_v	Vertical depression angle of line of sight along O-axis with respect to horizon.
N	Number of plane square segments required to partition the entire spherical visual field.
O-axis	Optical axis from eye normal to picture plane.
p	Sub- or superscript denoting aircraft-centered reference frame, aligned with direction toward ship.
r_o	Initial or average slant range along the O-axis to the (boresight) point of reference on the ship.
R	Slant range, sometimes with subscript m denoting range to target hover point.
s	Laplacian operator.
s	Sub- or superscript denoting ship-centered reference frame, aligned with earth frame of reference.
S	Ground range
T_G	Time advance providing perceptual preview
T/W	Thrust-to-weight ratio
U,V	Total velocity of aircraft
V_a	True air speed
V_G	Ground speed
V_s	Total velocity of ship
x	Longitudinal axis; also longitudinal displacement
y	Lateral axis; also lateral displacement or cross range
Y_v	Dimensional sway damping stability derivative (1/sec)
z	Right handed cartesian axis normal to xy plane; also corresponding displacement.
α	Angle of attack
β	Sideslip angle; also vertical depression angle of line of sight.
γ	Nominal glide slope angle
γ'_{h_o}	LOS_h
γ'_{v_o}	LOS_v

Γ	Angle defining direction of total velocity of aircraft with respect to x_E - axis.
$\Delta\psi$	Relative bearing of line of sight along O-axis with respect to aircraft nose.
ϵ	Small perturbation in the variable represented by subscript
θ	Perturbed pitch attitude of aircraft
κ	ℓ/a
λ	Meteorological back-scattering coefficient; also lateral coordinate of a point of regard in the field of view defined with respect to the O-axis, sometimes with subscript i.
μ	Vertical coordinate of a point of regard in the field of view defined with respect to the O-axis, sometimes with subscript i.
ν	Perceived inclination of the approach line-up center-line perspective angle with respect to horizon.
ξ	Perceived angle subtended at the eye by one-half of the hangar face width or height in Table 2.
π	3.14159....
σ	Koschmeider's meteorological extinction coefficient; also root-sum-squared or standard deviation, sometimes with subscript.
φ	Perturbed roll attitude of aircraft.
X	Approach bearing relative to ship in Figure 10.
ψ	Perturbed heading angle of aircraft relative to ship.
ω	Circular frequency, rad/sec.
Ω	Angular velocity.
$\dot{}$	(Raised period) differentiation operator with respect to time.
$\doteq$	Approximate equality.
$>$	Greater than.
$<$	Less than.

SECTION I

INTRODUCTION

At present there does not exist a rationale for specifying the requirements for forward field of view in an approaching V/STOL aircraft beyond that offered by pilot opinion of past practice (see Table 1, taken from Ref. 1), and simple considerations of aiming point visibility relative to approach path angle and vehicle pitch attitude. Roberts (Ref. 2) develops the latter methodology by considering the relationships between a fixed approach altitude and attitude, landing pad diameter (i.e., a delineation in the ground plane of the desired landing site), and the depression angle of the pilot's line of sight to the landing pad or over the nose afforded by the cockpit design. Missing from considerations such as these is a clear understanding of the possible tradeoffs among the various parameters affecting the approach situation. These parameters include the nominal or mean approach profile (flight path and speed as functions of range), the precision with which the pilot regulates the flight profile against disturbances (profile variability), visibility (considerations of VFR versus IFR, fog density, horizon visibility, texture cues), guidance and control cues afforded by the landing site (visual landing aids, pad shape, and illumination), and occlusion of the pilot's field of view by the cockpit canopy framing.

Although Thielges and Matheny (Ref. 3) attempt to analyze visual discriminations for helicopter control, unresolved questions remain concerning the way in which the authors of Ref. 3 applied Weber's Law for just noticeable differences to the apparent angular distances between internal referents on the cockpit canopy and external referents in the visual field on the ground plane. The present research addresses the subject in a somewhat different way, and is directly supportive of the upcoming development of the Navy's powered-lift flight technology.

TABLE 1

PILOT EVALUATION OF OUT-OF-COCKPIT VISIBILITY FOR V/STOL TASKS (FROM REF. 1 EXCEPT AS NOTED)

AIRCRAFT	PARAPHRASED PILOT EVALUATION
SC.1	Good downward view, particularly to each side of instrument panel
VAK-191B	Lookdown angle of 16 deg in landing attitude regarded as excellent for approach tasks; should be considered as a criterion for future designs
P.1127	Conventional fighter-type cockpit; special attention given to good visibility over the nose and sideways
XV-5A	(Army) Forward and sideward good; downward and aft restricted for hover and would be a shortcoming in an operational role (Air Force) Over the nose and downward not adequate for hover. Overhead restricted (painted to reduce heat load)
XC-142	Satisfactory in all respects except across cockpit and overhead (painted to reduce heat load). A visibility profile from the pilot's view point is presented in Fig. 1 projected on a picture plane from Ref. 2. Like flying in a goldfish bowl (second guessing at conclusions of project); would recommend modest and carefully considered reduction
CL-84	Satisfactory, but could be improved; over the nose barely adequate; over the side inadequate for SAR, adequate for normal approach
X-22A	Only 10 deg over the nose and insufficient for hover and low-speed flight research; improvement mandatory (a 5-inch full-width special instrument panel had been added)
AV-8A	Clear view of landing area is available during initial phase of decelerating transition. As aircraft nears termination of approach, landing area becomes totally obscured from pilot's view throughout hover at 50 ft above landing area. Visibility profiles from pilot's view point are presented in Fig. 2 projected on a picture plane (from Ref. 4) and in Fig. 3 projected on a 72 ft-square landing area from 50 ft hovering height (from Ref. 5). The pilot's forward view is restricted to a maximum downward visibility of 12 deg on the fuselage centerline and 42 deg downward at 65 deg right or left of the fuselage centerline.

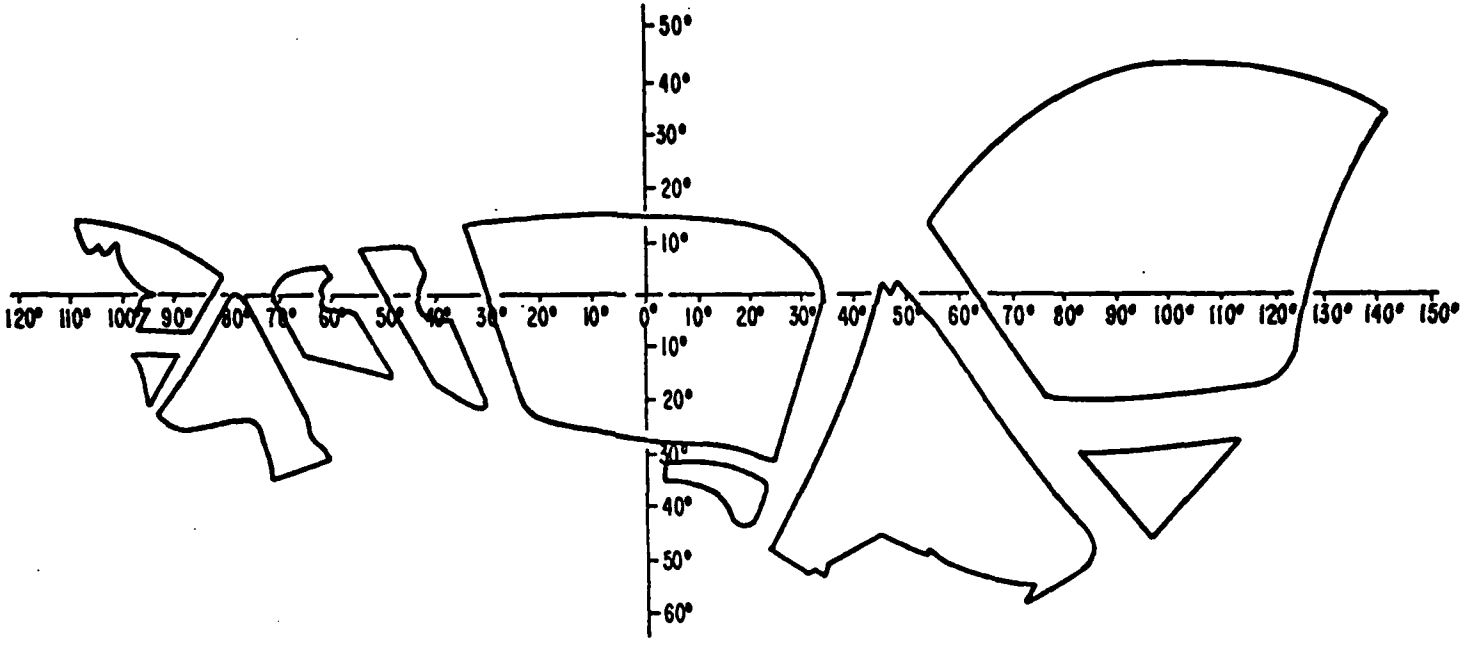

Figure 1. Picture Plane of XC-142 Cockpit Visibility (From Ref. 2)

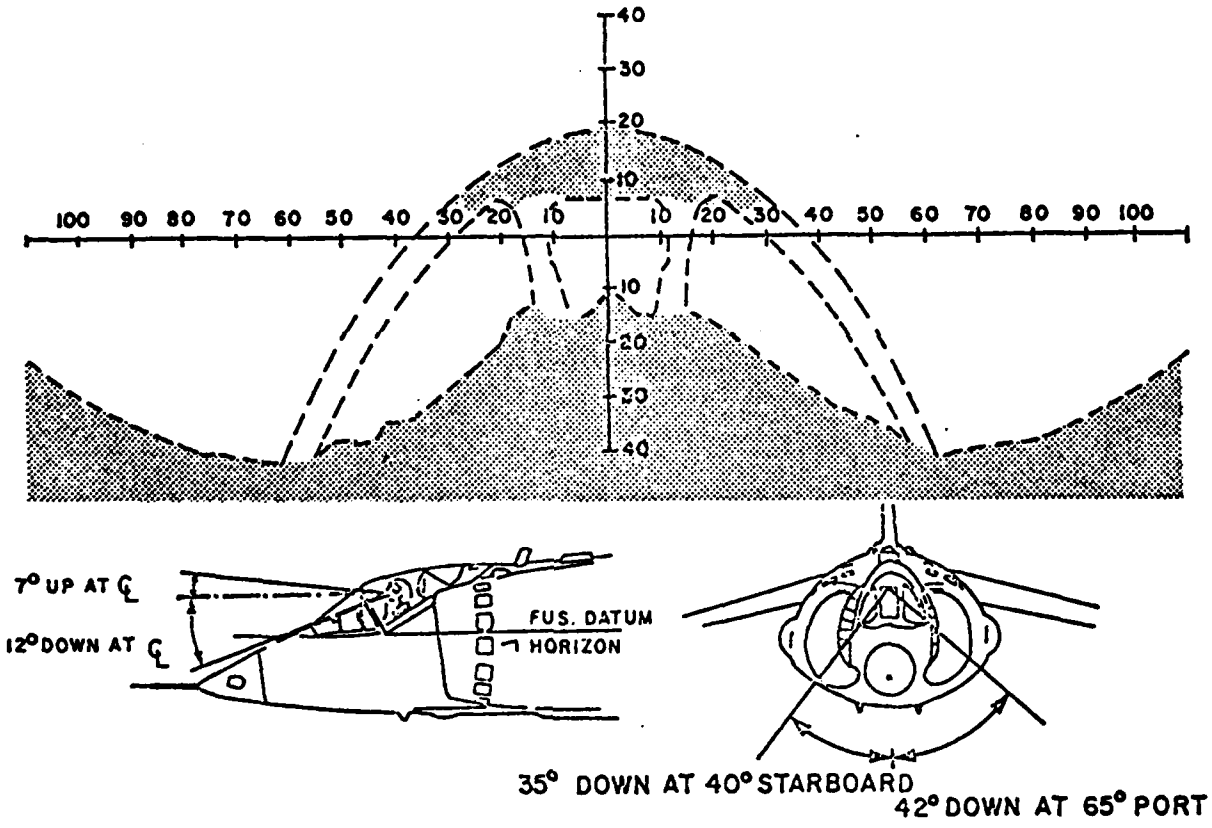

Figure 2. AV-8A Cockpit Field of View (From Ref. 4)

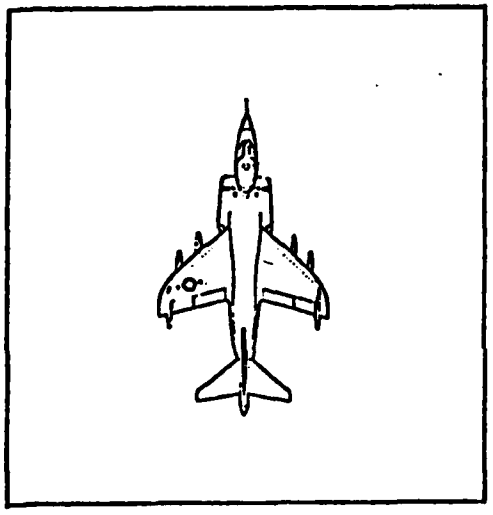

AV-8A AIRCRAFT ON 72' x 72' PAD

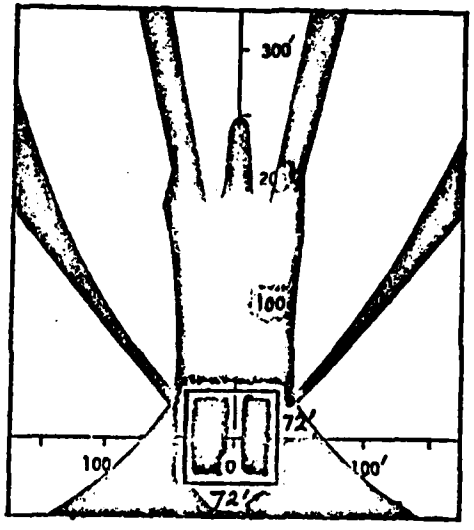

AV-8A PILOT'S VISION OBSTRUCTION
AT 50 FOOT HOVER

Figure 3. Cockpit Field of View Problem (From Ref. 5)

A. GOALS OF THE PRESENT STUDY

The purpose of this research is to develop and to quantify the needed rationale for fixed-wing V/STOL field-of-view requirements. The analytical technique is unique and involves the dynamic modeling of: a) the approach situation (including the pilot's control activities); b) the perceptual mechanisms of the pilot as affected by motion and visibility limitations; and c) the resulting apparent geometric forms, locations, angular sizes, and angular velocities relative to perceptual thresholds of informative elements within the visual field which provide guidance and control cues to the pilot. These are combined in the identification of those areas of the field of view which are essential for the perception of the cues for guiding and controlling the aircraft to a safe landing. What results is a synthesis of the disciplines of perception, guidance, and control based on external visual spatial and temporal cues. It then becomes possible to assess the relative merits of cockpit designs proposed for the V/STOL in terms of the occlusion of essential cues in the forward field of view.

B. BACKGROUND FOR THE PRESENT STUDY

Comprehensive expositions of the bases for understanding human visual perception of spatial and temporal surroundings were presented by Gibson (Ref. 6) in narrative form with propositions, axioms, and geometrical graphics which can be tested experimentally. Apparently motivated in part by a concurrent (circa 1950) survey of the status of research in visual perception by Graham (Ref. 7), Gilinsky (Refs. 8 and 9) developed and validated a quantitative formulation of visual size and distance perception. Gordon discussed human space perception mathematically in the context of the environmental geometry around a moving eye (Ref. 10) and set forth the perceptual basis of vehicular guidance (Ref. 11) in the vicinity of the ground plane.

The development of visual aids for conventional commercial aircraft approach guidance motivated Calvert (also circa 1950) to extend the theory of visual judgments of motion (Ref.12). Further insight for quantifying flight guidance and control by visual cues has been supplied by Havron

(Ref. 13), Naish (Ref. 14), and Grunwald and Merhav (Ref. 15). That portion of the theory which concerns the acquisition of position and velocity information will be applicable to the present study; however, our interest in the field of view will necessarily focus on the latest stage of the approach prior to hovering flight where the apparent relative size of the landing pad is great but where the relative velocity between aircraft and landing pad may be so low as to inhibit the perception of "streamers" which otherwise play a more significant role in conventional visual landing guidance. Consequently for the present study we shall borrow from the theory of visual perception chiefly those essential geometrical constructs and relationships which describe relative position between aircraft and landing pad and which are summarized in Table 2 in terms of the ship's deck pad and hangar delineation.

Perfect recognition by the pilot of the ship's deck delineation and landing aids which are necessary for guidance and control of the aircraft approaching the landing pad is an idealization of reality even though in the approach and landing task the experienced pilot must recognize only very familiar memorized geometric patterns. Thus in terms of the successive organization of perception theory (Ref. 16) and the sequential theory of pattern perception in Ref. 17, the pilot is probably always operating at the pursuit level of pattern perception, where it may be reasonable to assume that recognition is conditioned only upon detection with fairly high probability, say 0.95, and insignificant additional time delay over that already accounted for in the effective perceptual-motor delay, τ_e, of the crossover model for the compensatory level of control, unless head movements are required to scan the functional visual field as defined, for example, by Sanders' selective process (Ref. 18).

Sanders has shown in a decade of visual research at the TNO in Holland (Ref. 18) that a "scanning controller" function exists which directs the motions of the eye and head to points of interest in the visual field. For cues at angles from the foveal axis of less than about 20 deg, the eye need not, but may, be moved; for angles between 20 and 60 deg only the eye is moved in one dominant saccade at a slew rate on the order of 300 deg/sec. For points-of-interest further than 60 deg, the head is moved as well, thus requiring more time to complete the saccade.

TABLE 2

EXAMPLES OF VISUAL POSITION CUES PROVIDED TO THE APPROACHING PILOT BY THE GEOMETRY OF THE SHIP'S DECK PAD AND HANGAR DELINEATION

COORDINATE OF POSITION	RATIONALE FOR DELINEATION	CUE PROVIDED BY DELINEATION	TYPICAL VIEW OF DELINEATION	PREFFERRED VIEW OF DELINEATION FOR HOVERING	APPARENT SENSITIVITY OF DELINEATION GEOMETRY
Longitudinal Position in Approach	Necessary for approach guidance, especially at low speeds	Apparent size of hangar/deck/pad/VIA	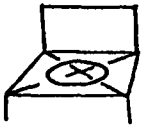 See also sketch at bottom of column for close-up	See sketch below	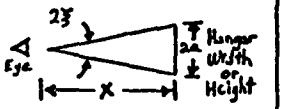 $\frac{\partial \xi}{\partial(\frac{x}{a})} = -\sin^2\xi$ becomes greater as $\xi \rightarrow \pi/2$
Longitudinal or Lateral Position in Hovering	Necessary for approach, hovering and landing line-up guidance	Apparent differential in depression angle of deck outline relative to ship's superstructure or horizon, if visible Hovering PPI is a candidate for VIA	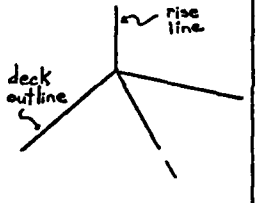	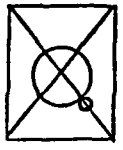 (Hovering PPI is a candidate for VLA)	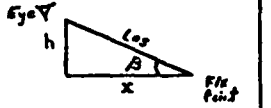 $\frac{\partial \beta}{\partial(\frac{x}{h})} = \sin^2\beta$ becomes greater as $\beta \rightarrow \pi/2$
Lateral Position in Approach	Necessary for line-up guidance	Apparent inclination of symbology representing deck/pad line with respect to drop/rise lines	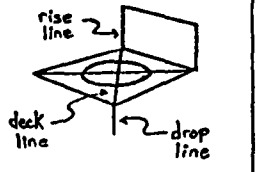	See sketch above	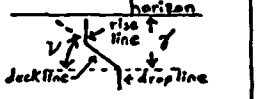 $\frac{\partial \nu}{\partial(\frac{y}{s})} = -\cot\gamma \sin^2\nu$ becomes greater as $\nu \rightarrow \pi/2$, i.e., when aligned. s = range-to-go, y = lateral offset from deckline extension
Normal or Vertical Position	Necessary for approach, hovering and landing guidance in a vertical plane	Glide slope deviation would be provided by VIA during approach Altitude itself is provided in terms of hangar and superstructure during hovering Apparent size of deck outline or apparent depression angle of deck outline also provides height cue	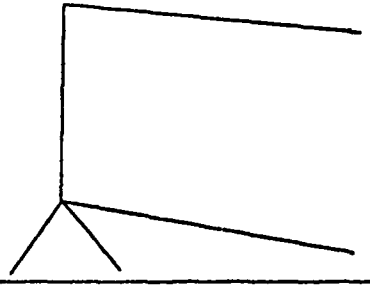		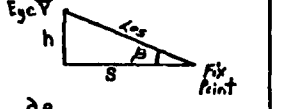 $\frac{\partial \beta}{\partial(\frac{h}{s})} = \cos^2\beta$ becomes greater as $\beta \rightarrow 0$

Numerous experiments (Refs. 19-21), using eye and head point-of-regard instrumentation, have shown that both the eye and head tend to move in a series of very sharp saccades (steps) while changing one's point-of-regard. The resulting image blur during a saccade is suppressed internally by a feedforward signal from the eye movement controller, so that perception is briefly lost during each saccade. Thus, the net effect on the perception of a cue's form or motion is a short average delay due to scanning saccades.*

A typical nighttime appearance of a pad and hangar is presented in Fig. 4 with permission from Ref. 22. Most apparent are the contrasting photometric properties between the white hangar floodlights and darker (red) deck and hangar flood lights which help to define the recovery area itself. The other important elements in the visual field from the pilot's point of view are the changing geometric properties of the deck and hangar delineation lights, deck line-up lights, drop lights, and visual landing aids such as the glide slope indicator illustrated above the port corner of the hangar. Other visual elements of significance to the pilot, but not shown in Fig. 4, are the red flood-lighted superstructure above the hangar. The surpassing importance of the superstructure for hovering and near-hovering guidance and control cues is revealed by the pilots' flight test reports in Refs. 23 and 24.

Perception of the changing geometric properties, however, is conditioned upon the perceived photometric properties, such as illuminance, reflectance, and color, which will be altered by environmental attenuation and scattering. At the relatively short visual ranges to the deck from hovering and near-hovering positions, scattering is the predominant effect at night. Scattering acts to reduce contrast and to desaturate colors (Ref. 25). Backscatter from landing lights on the aircraft, intermittent attenuation

---

* The details of the intentional movement dynamics of both the head and eye are fairly well known and are quite complex in detail (e.g., Ref. 21). However, because the saccades are rapid (less than 0.06 sec for eye-only motions), for purposes of analysis and evaluation the effect can be represented by a delay in perception of displayed states. This delay can be lumped with a typical detection delay of about 0.02 sec.

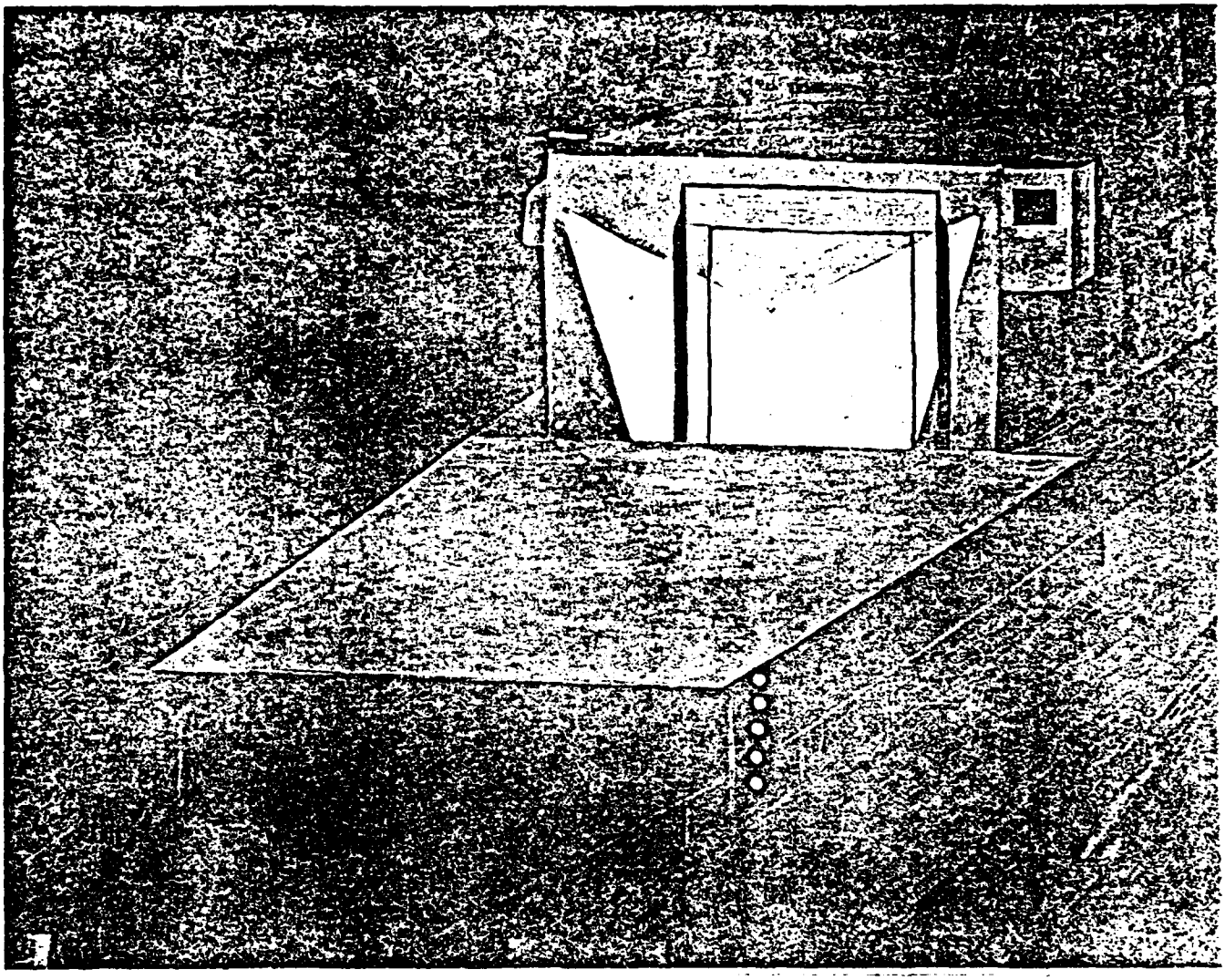

Figure 4. V/STOL Night Approach Scene
(Reproduced from Ref. 22 with permission from the copyright owner)

from sea spray, and the possibility of reflected glare from white flood lights provide a complex distribution of veiling luminance in the external field of view at night. Scattering and attenuation increase with the density of precipitation (e.g., rain, sea spray, fog) and the range of the observer from the ship.

Luminant source attenuation effects, which predominante in daylight, have been described by the Koschmeider theory (Ref. 25). The effects of backscatter and glare at night cause the inherent contrast of a luminant source to attenuate more rapidly than is described by the (exponentially) linear relationship with range identified as Koschmeider's law (Ref. 26). The effects of backscatter and glare can, however, be imbedded in a modification of Koschmeider's law by representing the exponent as a truncated power series in range, R*.

Allen and McRuer (Ref. 27) have coupled the modified Koschmeider theory with the modified Blackwell-Davies contrast thresholds (Refs. 28, 29, and 30) in studies of how the visual segment can affect perceptual cues for guidance and control of surface vehicles. The same technical approach has been applied in Ref. 31 to estimate the minimum effective visual range for guidance and control of VTOL operations at night, if the minimum visual range in daylight is 700 ft as proposed in Ref. 5. At a visual range of 300 to 400 ft or greater at night it appears that the contrast threshold may inhibit perception of floodlighted painted deck markings, even though the high-intensity delineation lights and visual landing aids will be visible. For hovering near the ship in sea spray at night within 300 to 400 ft visual range, we may therefore expect that the contrast threshold will have only an intermittent impact on perception of the darker (red floodlighted) painted deck markings. Thus our divided or intermittent

---

* The observed luminance contrast C_R, at range, R, is given by

$$C_R = C_o \exp(-\sigma R - \lambda R^2 - \ldots)$$

where C_o = inherent source or target contrast
σ = Koschmeider's meteorological extinction coefficient
λ = backscattering coefficient

attention models for perception (Ref. 16), coupled with Gilinsky's models for the perception of size and distance (Refs. 8 and 9) should be adequate for application in the guidance and control analysis (Refs. 32, 33, and 34) for the present study.

C. SENSITIVITY OF VISUAL CUES IN VTOL APPROACHES

We have already presented in Table 2 the key roles for visual cues in VTOL approaches. In this topic we shall introduce a measure of sensitivity which affects the pilot's perception of those essential geometric properties of pad delineation and visual aids, which provide position information and also are summarized in Table 2. The changing aspects of pad delineation from several nominal approaching trajectories will be presented in more detail in Section III after we have compared several trajectories in Section II.

The possibility of instrument to visual transitions requiring a wide parafoveal — even peripheral — awareness of the ship's hangar and pad position cues is apparent from the nighttime appearance in Fig. 4. When the angular regions in the field of interest defined by Sanders' selective process (p. 7 herein) are considered, it is clearer why pilots may experience significant workload in acquiring external visual cues close to the ship. Experimental work reported in Ref. 35, while applied to automobile driving, confirms that the use of small aperture viewing (without correspondingly improved viewing resolution) is reported to cause increased workload, suggesting that denial of the peripheral cues may lead to significant degradation in the perceptive structure.

1. Considerations for Vertical Displacement Control

Expressions are shown in the extreme right column of Table 2 for the sensitivity of the line of sight depression angle, β, to changes in ground position, x, and height, h. The advantage of the constant path angle approach to the pad to be discussed in Section II is the compensatory guidance and control feature of the pad appearance at constant depression angle. The superior altitude sensitivity of pad depression angle on shallow path angle approaches is evident from the expression for $\partial\beta/\partial(h/s)$

in Table 2 where the sensitivity decays as the square of the cosine of the depression angle of the line of sight to the pad. The altitude sensitivity is quite acceptable over the range of relatively shallow approach angles to be considered in Section II.

In contradistinction, the sensitivity of lateral and longitudinal ground position cues while in hover and near transition to hover is unfortunately best at large depression angles near the nadir. Field of view at these angles is nearly impossible to provide in aircraft. However, it underscores the need to keep the instrument panel from growing out of bounds where it will deny the essential peripheral vision at large line of sight depression angles. Again, hover position sensitivity perceived by the pilot falls off to about half its maximum value as the line of sight rises to 45 deg depression. The two-fold change in ground position sensitivity while on VFR is most important when synthesizing a hover position control display for a visual landing aid or for a head-up display. We have seen a variety of simulated plan position indicators which present the nadir view of the pad in relation to the aircraft or the aircraft in relation to the pad. While using such an instrument, the pilot has the advantage of maximum longitudinal and lateral displacement sensitivity over the ground, yet when he seeks the transition to visual contact, his line of sight depression angle to the hangar or pad may be much less than 45 deg. On acquiring the hangar or pad visually, the pilot may discover that the displacement sensitivity is less than half that which he was accustomed to on instruments. Thus, the pilot is suddenly required to adapt his loop gain to the change in perceived displacement sensitivity. Although a 3 or 4 fold increase in pilot gain is quite possible, the IFR/VFR transition point is a very unfair place to require it, since the pilot is preoccupied with vehicle trim changes and with the transition to hover for the unforgiving vehicle itself.

2. Considerations for Lateral Displacement Control

Consider the pilot's view of the landing pad centerline as seen from a point short of the pad and displaced to the left. Geometrically, the situation is as shown in the left portion of Fig. 5, with the pilot's eye

γ = Nominal Glide Slope Angle

ν = Approach Line Up Centerline Perspective Angle

y = Lateral Displacement

h = Altitude

$\overline{F_1F_2}$ = Line Up Centerline

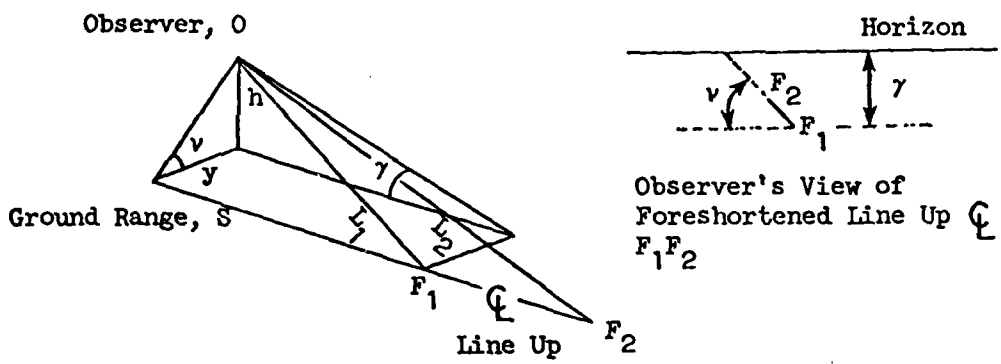

Figure 5. Geometry for Perception of Time-Advanced Lateral Deviation

view shown on the right. The sensitivity of the perspective angle, ν, to changes in lateral displacement, y (with the latter normalized by the ground range, S) is equivalent to the partial derivative, i.e.,

$$\frac{\partial \nu}{\partial (y/S)} = - \cot \gamma \sin^2 \nu$$

This sensitivity is greatest at shallow depression angles (small γ) when ν is near 90 deg, i.e., when nearest to being lined up with the pad centerline. It falls to half of this value for ν = 45 deg and decreases rapidly toward zero for decreasing ν. The strong lateral displacement or line-up cue provided by the line-up centerline and drop line lights is also evident in Fig. 4.

One way in which the line-up centerline displacement cues can provide for adoption of an advantageous lateral displacement loop-structure on the part of the pilot is shown in Appendix A. The perspective angle of the line-up centerline in combination with its time rate of change provides an effective time-advanced lateral deviation (Ref. 36). Preview is explicit in this case simply by viewing the perspective angle of the centerline, and associating this angle with the lateral position error that the vehicle would have at some point ahead of the vehicle if it continued along its current path. This is illustrated in Appendix A, where the ground range to the point of regard is given by S, which is approximately equal to the relative closing velocity, V_G, multiplied by the time, T_G, to travel to that point. The time advance, T_G, provides a perceptual preview which results in a pure-lead equalization in the effective controlled element dynamics. This, in turn, offsets the undesirable K/ω^2 form of the lateral deviation dynamics at low frequency.

The point of all this is to demonstrate that the pilot's perceptions of changes in altitude (h), cross range (y), and ground range (S) errors are functions of where the visual field elements are located in his field of view (β and ν), in this instance, all on the (approximately horizontal) plane representing the deck's surface. Further, these functions can be explicitly quantified. The scope of this study is to develop similar measures of visual element (e.g., the landing pad centerline, the drop line, and the hangar face) changes with vehicle motions, and various

disturbances; and to relate these measures of change to the pilot's ability to perceive or discriminate the change (e.g., cockpit framing occlusions, haze, fog, sea spray, and confusing factors such as angular motion perturbations of the V/STOL aircraft, and motions of the ship).

D. SCOPE OF THE PRESENT STUDY AND PROCEDURE FOR DETERMINING EXTERNAL VISUAL FIELD OF VIEW REQUIREMENTS

In this topic we shall describe the scope of the present study by outlining the procedure which we have evolved for determining external visual field of view requirements. Each of the four major steps in the procedure will be described briefly and partitioned into subsidiary tasks, for which there are six supporting working papers to help the interested analyst in carrying out the technical details. The six working papers are identified by their "WP-number," and their full titles are listed on p. 20. The interactive procedure for determining field of view requirements presently also includes two small HP-67/97 computer programs supplied with the corresponding working paper to aid the analyst. The six working papers can be obtained at cost from the technical librarian of Systems Technology, Inc.

Step I — Kinematic Representation of Aircraft Approach Trajectories to a Landing Pad on a Moving Ship or Shore-Based Site (WP-1122-1)

The first step in the procedure is to define the intended approach trajectory of the aircraft with respect to the recovery area on a moving ship or shore-based site. (In this study, we have addressed the more general problem of recovery on a moving ship). The pertinent coordinate transformations and kinematic relationships for a point-mass aircraft are employed. The results of this step are described in Section II of this report and include the sequence of nominal operating points in terms of range, bearing, and altitude with respect to the terminal hovering point over the pad as a function of time. The specific tasks for this step require that the analyst:

a. Specify ship velocity, if appropriate; specify desired type of approach trajectory, deceleration, and terminal hovering coordinates

of aircraft. Reference 37 and p. 420 of Ref. 38 may be consulted for details of ship's recovery area geometry.

b. Define position coordinates of a point-mass aircraft relative to the terminal hovering point over the pad as a function of time (HP-67/97 program is available for constant relative bearing, rectilinear, and constant sink rate; Tymshare PDP-10 program, for homing).

Step II — Pilot/Vehicle Performance

The second step in the procedure is to estimate what effects pilot-controlled vehicle (rigid-body) motions about the vehicle center of mass will have on perturbations in following the sequence of operating points during the course of a typical approach. This requires the quantification and exercising of an analytical model of the pilot-plus-vehicle executing the intended approach trajectory under the influence of turbulence, ship motion, degraded visibility, and pilot variability (e.g., as caused by divided attention to several control and monitoring tasks during the approach). The results of this task are quantitative relationships between the trajectory variables, ship motions, turbulence, and piloting noise on the one hand and the variability in the angular and translational kinematics of the aircraft on the other. The results of Step II are described in WP-1115-5 and are applied to Step III by example in Section III of this report. The specific tasks for Step II require that the analyst:

a. Define the aircraft control problem and task in terms of:

   forcing functions, task and outer-loop variables,
   controlled element transfer functions (WP-1115-1),
   and performance (error) requirements (WP-1115-5).

b. Prepare a prospectus of control loops by numerator inspection and select candidates for inner loops associated with outer (task) loops from Step a (WP-1115-1).

c. Establish stability margin requirements from crossover model (WP-1115-1).

d. Analyze control loops using adaptive feedback selection hypothesis to determine: selected automatic, visual, and other multimodal feedbacks (constituent cues or signals, reference systems, and necessary equalization), piloting techniques, describing functions, sources of pilot remnant (e.g., observation thresholds, equalization and processing, and division of attention) (WP-1115-5).

e. Compute effective division of attention among control axes which minimizes total error vector for assigned levels of observation thresholds*, equalization, and processing noise. Reiterate from Step c, if necessary. (WP-1115-5).

f. Compute coherence determinant and test for reasonability (WP-1115-5).

g. Compute input-correlated and root-sum-squared error vector (WP-1115-5).

h. Compute total root-sum-squared error vector and compare with performance requirements. Reiterate from Step e, if necessary (WP-1115-5).

Step III — Visual Element Motion Analysis

The third step in the procedure is to convert the sequence of operating points along the approach trajectories, as well as the perturbations about these trajectories, into corresponding apparent angular kinematics ascribed to a set of representative visual elements in the pilot's external field of view. In this study the representative visual elements will be the deck pad and hangar delineation for a DD963 class of destroyer (Ref. 37 and p. 420 of Ref. 38), which has a 40 ft-by-60 ft recovery area and a 40 ft wide-by-20 ft high hangar face. The results of Step III are presented in Section III of this report. The specific tasks for Step III require that the analyst:

a. From the sequence of nominal trajectory operating points in Step I, identify geometric forms (and their sensitivity functions)

---

* Observation thresholds are based on contrast, visual acuity, and indifference thresholds in Step IIIa.

of essential elements in the visual field which provide cues for outer loop task variables as a function of meteorological conditions which affect contrast and visual acuity (WP-1115-3). Reference 37 may be consulted for details of recovery aids and area geometry.

b. By means of the necessary coordinate transformations and kinematic representations, relate nominal aircraft trajectory motions in Step I and positions to angular motions and positions of referents in the pilot's forward visual hemisphere (WP-1115-2 and HP-67/97 program). The advantages and disadvantages of polar and cartesian picture planes for this step are discussed in Appendix B. We have used the cartesian picture plane in this study.

c. By means of perturbed linearized coordinate transformations and kinematic representations, relate disturbances in ship and aircraft motions and positions to variability in the nominal angular motions and positions of referents in the pilot's forward visual hemisphere (WP-1115-4).

d. Superimpose angular measures of variability (e.g., root-mean-squares) in Step c on nominal motions and positions of referents in Step b (WP-1115-4).

e. Partition contributions to variability from ship motion, atmospheric turbulence, and pilot-induced noise in Step II (WP-1115-5).

Step IV — Field of View Requirements

Combining in Step IIId the "nominal" angular motions and positions of essential referents from Step IIIb with the estimates of variability in these same nominal motions and positions from Step IIIc allows the analyst to define explicitly the location of essential visual cues (for guidance and control of the aircraft) within the pilot's forward visual hemisphere from which field of view requirements can be established. Furthermore the source of each contribution, whether nominal or variable with some probability, can be identified. Thus, similarly appearing variations with different causes could be identified as potential sources of ambiguity in interpretation. The concluding assessments of field of view requirements from the

examples examined in this fourth step are presented in Section IV of this report. The specific tasks in Step IV require that the analyst:

a. Establish probable bounds on the forward hemispheric field of view which includes the essential cues and referents from Step III, Step d.

b. Based on the apparent geometric sensitivity functions (Step III, Step a) and the acceptable range of the pilot's gain adaptation, estimate the comparative usefulness of the available cues for the guidance and control of the aircraft; and identify essential areas within the probable bounds on the field of view from Step a for perception of guidance and control cues.

c. Estimate minimum field of view boundaries which include essential areas.

d. Compare results with typical cockpit occlusions and fields of view for head-up displays.

A list of working papers which describe the technical details of each step follows.

WP-1115-1, "Development of General Closed Loop Pilot Vehicle Dynamics for VTOL Aircraft at Low Speeds"

WP-1115-2, "Computation of the Pilot's View of a Non-Aviation Ship's VTOL Pad for Several Types of Approach Trajectories"

WP-1115-3, "Some Effects of Adverse Visibility on Threshold Properties of the Pilot's Perception in VTOL Approaches to Non-Aviation Ships"

WP-1115-4, "Perturbations of the Pilot's View of a Non-Aviation Ship's VTOL Pad Due to Linear and Angular Perturbations of the Aircraft"

WP-1115-5, "Linear and Angular Perturbations of Piloted VTOL Aircraft at Low Speeds Caused by Ship Motion, Atmospheric Turbulence, and Pilot-Induced Noise"

WP-1122-1, "Computation and Analysis of V/STOL Approach Trajectories"

SECTION II

COMPARISON OF V/STOL APPROACH TRAJECTORIES

This section compares six general types of V/STOL approach trajectories to a moving ship from Ref. 34. Included in this section are trends in field of view requirements among the following types of trajectories:

- Constant bearing
- Rectilinear
- Homing
- Constant sink rate
- Constant altitude
- Velocity proportional to perceived range

Trajectories in the horizontal and vertical planes are considered separately, i.e., the trajectories are only two-dimensional. The method used in Ref. 34 to derive the equations, however, lends itself to easy implementation of three-dimensional equations if desired.

A. HORIZONTAL PLANE RELATIONSHIPS

The trajectory equations are based on the Coriolis law:

$$\frac{d}{dt}\vec{R}^{E} = \frac{d}{dt}\vec{R}^{P} + \vec{\Omega}^{P/E} \times \vec{R}$$

Four reference frames are involved:

B — Aircraft centered, aligned with total velocity, U

P — Aircraft centered, aligned with direction toward ship

E — Aircraft centered, aligned with earth frame

S — Ship centered, aligned with earth frame.

Figure 6 shows the reference frame relationships and defines key quantities. The subscript h refers to the horizontal plane; however, the subscript will be dropped from the equations in Table 3 for simplicity, because the same equations in Table 3 apply to analogous relationships in the vertical plane as well. The ship velocity in the earth frame is assumed constant.

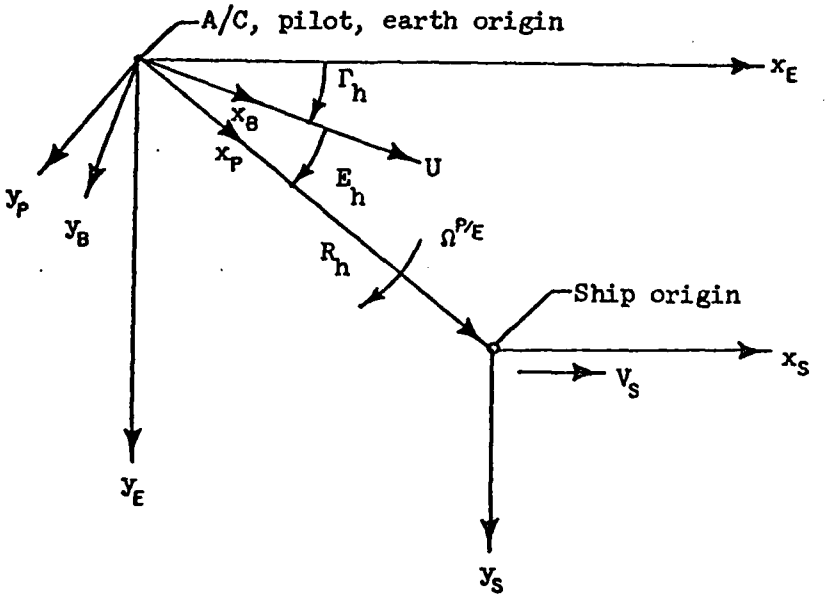

Figure 6. Horizontal Plane Relationships.

B. VERTICAL PLANE RELATIONSHIPS

Trajectory equations in the vertical plane can be formulated by direct analogy to the horizontal plane. The diagram in Fig. 7 shows the vertical plane relationships. The aircraft origin is drawn below the ship only to preserve a right hand rule; in practice the relative bearing, $\Gamma_v + E_v$, is always negative.

C. CLASSIFICATION OF TRAJECTORIES

Six special kinds of trajectories are considered here:

- A trajectory which maintains a constant bearing with respect to the ship — $E + \Gamma$ = constant (such as a

	CONSTANT BEARING	STRAIGHT LINE PATH
Special Conditions	$E + \Gamma = E_o + \Gamma_o$	$\Gamma = \Gamma_o$
Range Rate Equation	$\dot{R} = V_s \cos(E_o + \Gamma_o) - U \cos E$	$\dot{R} = V_s \cos(E_o + \Gamma_o) - U \cos$
Angular Relationship	$E = \arcsin \frac{V_s \sin[E_o + \Gamma_o]}{U}$	$\dot{E} = -\frac{1}{R}[V_s \sin(E + \Gamma_o)$ $- U \sin$
Normal Acceleration	$U\dot{\Gamma} = \dot{U} \tan E > \dot{U} \sin E$ $= \frac{\dot{U}}{U} V_s \sin[E_o + \Gamma_o] < 0$	$U\dot{\Gamma} = 0$
Total T/W	$(T/W)^2 \doteq 1 + \left(\frac{\dot{U}}{g}\right)^2 - 2\frac{\dot{U}}{g}\frac{\sin(E_o + \Gamma_o)}{\cos E}$	$(T/W)^2 \doteq 1 + \left(\frac{\dot{U}}{g}\right)^2 - \frac{2\dot{U}\sin$ g

TABLE 3

SUMMARY OF TRAJECTORY TYPES

STRAIGHT LINE PATH	HOMING	CONSTANT SINK RATE	CONSTANT ALTITUDE	VELOCITY PROPORTIONAL TO PERCEIVED RANGE
$\Gamma = \Gamma_o$	$E = 0$	$U \sin \Gamma = \text{const}$	$\Gamma = 0$	$\dot{R} = -K_t R/(1 + R/A), \quad \dot{\Gamma}+\dot{E} = -K_n(\Gamma+E)/(1 + R/A)$
$\cos (E_o + \Gamma_o) - U \cos E$	$\dot{R} = V_s \cos \Gamma - U$	$\dot{R} = V_s \cos (E+\Gamma) - U \cos E$	$\dot{R} = (V_s - U) \cos E$	$\dot{R} = V_s \sin (E+\Gamma) - U \cos E$
$[V_s \sin (E + \Gamma_o)$ $- U \sin E]$	$\dot{\Gamma} = -\frac{1}{R} V_s \sin \Gamma$	$\dot{E}+\dot{\Gamma} = -\frac{1}{R} (V_s \sin (E+\Gamma) - U \sin E)$	$\dot{E} = -\frac{\dot{R}}{R} \tan E$	$\dot{E}+\dot{\Gamma} = -\frac{1}{R} [V_s \sin (E+\Gamma) - U \sin E]$
$U\dot{\Gamma} = 0$	$U\dot{\Gamma} = -\frac{UV_s}{R} \sin \Gamma < 0$ (always concave away from ship $\mathcal{C}_L$)	$U\dot{\Gamma} = -\dot{U} \tan \Gamma > 0$	$U\dot{\Gamma} = 0$	$U\dot{\Gamma} = f(R, A, K_t, K_n)$
$+\left(\frac{\dot{U}}{g}\right)^2 - \frac{2 \dot{U} \sin \Gamma_o}{g}$	$(T/W)^2 \doteq 1 + \left(\frac{\dot{U}}{g}\right)^2$ $- 2\left(\frac{\dot{U}}{g} - \frac{UV_s}{R}\right)\sin \Gamma$	$(T/W)^2 \doteq 1 + \left(\frac{\dot{U}}{g}\right)^2$	$(T/W)^2 \doteq 1 + \left(\frac{\dot{U}}{g}\right)^2$	Not Derived

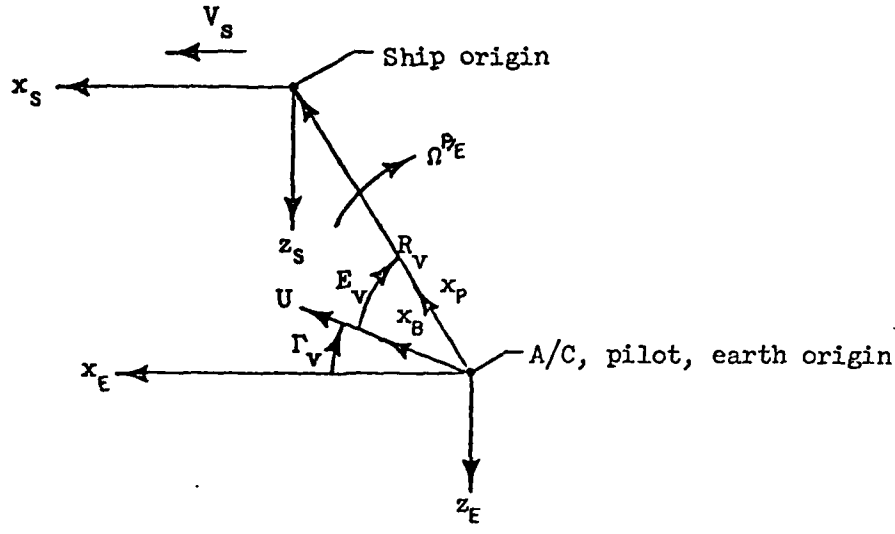

Figure 7. Vertical Plane Relationships

conventional approach using fixed line-up and glide slope angles)

- A trajectory which follows a straight line path in the earth frame — Γ = constant
- A homing trajectory in which the aircraft flight path vector is always pointed toward the ship — E = 0
- A constant sink rate trajectory (at constant horizontal bearing) where acceleration along the earth x-axis is constant
- A constant altitude trajectory where acceleration along the earth x-axis is constant
- A variable deceleration trajectory in which inertial velocities tangent and normal to flight path are proportional to visually perceived position — a trajectory which closely approximates manual, head-up approaches to hover.

The resulting trajectory equations for each of the above cases are summarized in Table 3.

1. Trajectories in the Horizontal Plane

A typical V/STOL approach to an aviation facility ship can be characterized in the horizontal plane by one of the graphs in Fig. 8 in terms of a curvilinear course from either stern quarter, although Fig. 8 shows trajectories from only the starboard quarter in the ship's reference frame. Thus, the straight line trajectory (in inertial space) appears curved and the constant bearing trajectory (in the ship's reference frame) appears straight.

The main feature of the straight line approach is that it terminates from abeam the ship while the homing terminates from astern. Termination could be from any arbitrary angle if transition to a constant bearing trajectory were implemented. (The initial relative bearing angle, $\Gamma_h + E_h$, may be between 25 and 45 deg with respect to hull centerline, depending on the ship's recovery pad marking.) On a constant bearing the approaching aircraft must not only cope with a crosswind component but also fly a curved course in pursuit of the recovery pad on the moving ship as the aircraft decelerates. The pilot of the aircraft must therefore adopt either an increasing crab angle equal to E_h, if side slip angle $\beta = 0$, or a decreasing bank angle shown in Fig. 8, if $\beta = E_h$, as his relative speed drops. Either technique poses questions about field of view, although the decreasing bank angle probably interferes less with hovering and recovery field of view. Although one could, in principle, revise the relative course of the ship to minimize the crosswind component encountered by the aircraft, this will not necessarily help the pilot either, because he would then encounter air turbulence induced by the ship's superstructure throughout the approach.

2. Trajectories in the Vertical Plane

A typical V/STOL approach trajectory can be characterized in the vertical plane by the graphs in Fig. 9, in terms of a curvilinear terminal

All trajectories start at:

$U = 100$ kt

$\Gamma+E = 30$ deg

and end at:

$U = V_s = 20$ kt

$\Gamma = 0$

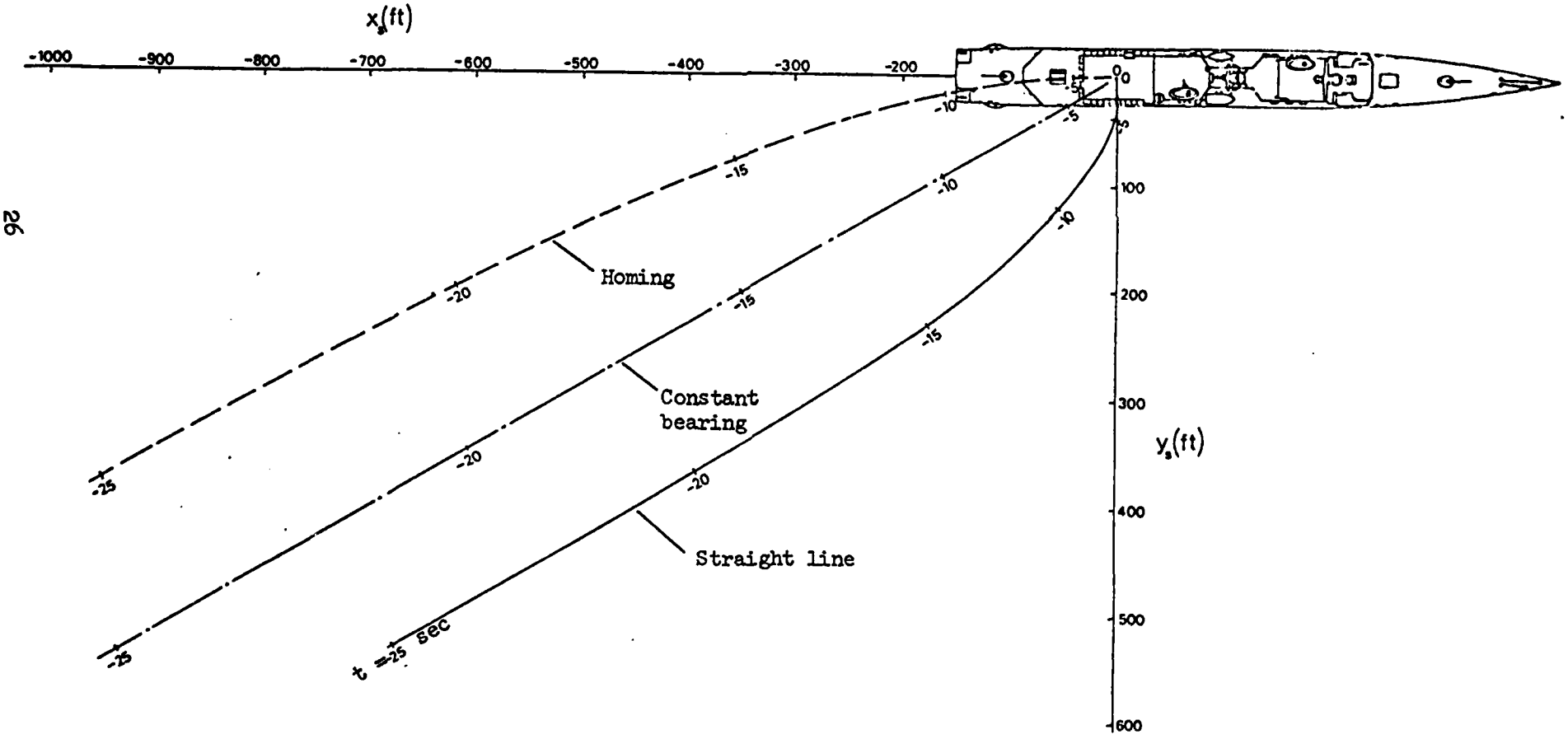

Figure 8. Horizontal Plane Trajectories in Ship Frame

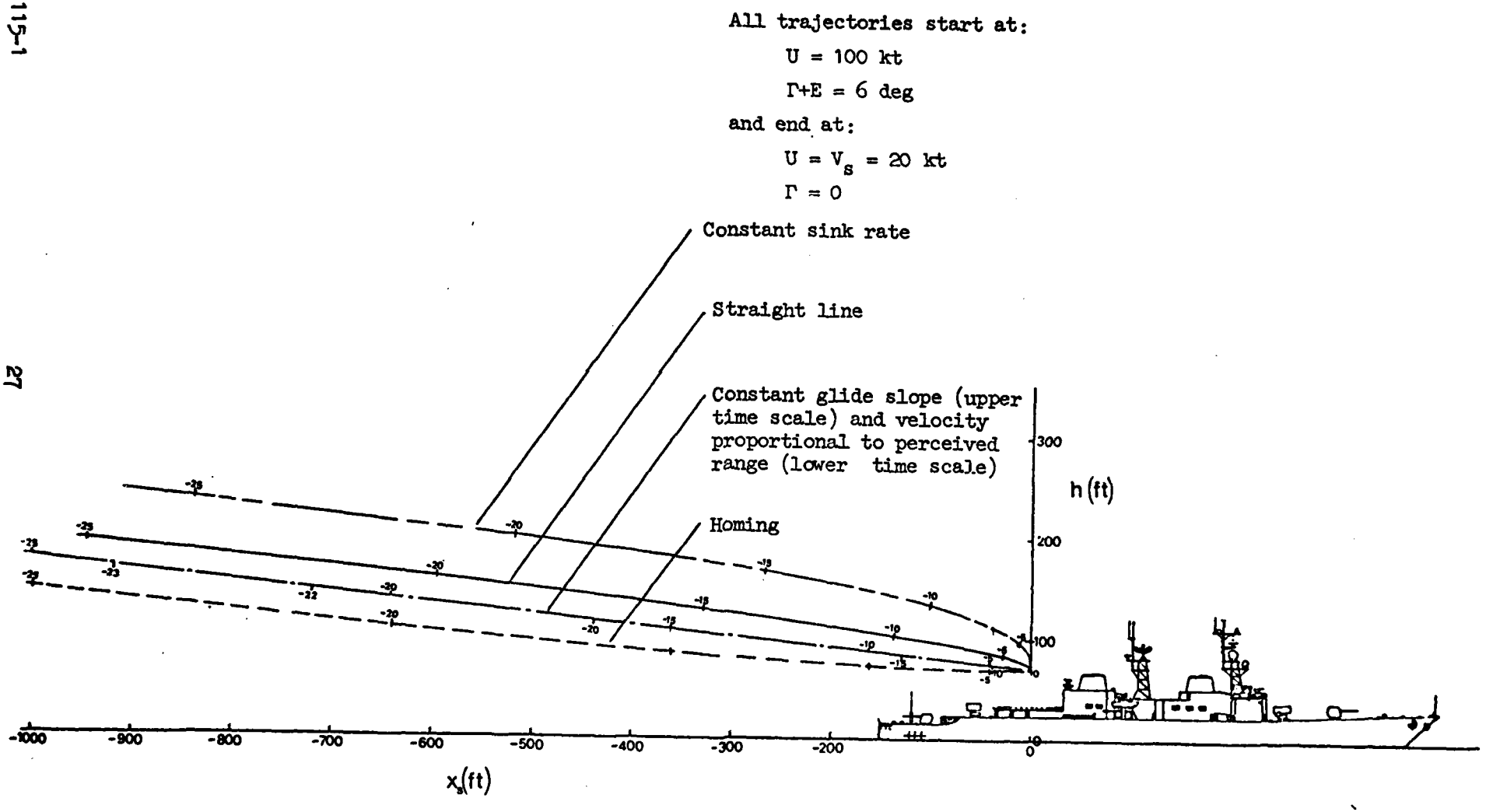

Figure 9. Vertical Plane Trajectories in Ship Frame

glide path angle to the hovering condition. (The initial relative elevation angle $\Gamma_v + E_v$ has been chosen as -6 deg to accommodate the constant deceleration of 0.1 g.) Even shallower glide slopes may be necessary in cases where the aircraft's deceleration control is authority-limited. The constant glide path type of trajectory has been designed so that some of the regulated variables in the vertical plane (e.g., speed, glide path displacement, and pitch attitude) may be as non-interacting as possible in view of the need for decelerating speed and adjusting trim controls during the conversion to the hovering condition. Velocity proportional to perceived range can be slightly concave upward (like the straight line trajectory) or downward (like the homing trajectory) but is nominally close to a constant glide slope trajectory. The time dependence is, however, significantly different owing to the variable deceleration.

D. AIRCRAFT-TO-SHIP (FIELD OF VIEW) ANGLES

The aircraft-to-ship field of view relationship depends not only on trajectory type but also on how the aircraft is oriented with respect to its flight path vector. If the aircraft's x-axis is aligned with the ship's x-axis ($\theta = 0$ or $\psi = 0$) then the aircraft-to-ship relative angle is Γ+E. But, if the aircraft's x-axis is aligned with its flight path ($\alpha = 0$ or $\beta = 0$) then the aircraft-to-ship relative angle is E. Hence, in the former case the figures showing Γ+E versus R are more relevant for the vertical plane relationships and in the latter case the graphs showing E versus R are more relevant for the horizontal plane relationship if $\beta = 0$. (Recall that, if $\beta = E$ in the horizontal plane, Fig. 10 shows the bank angle required to keep the aircraft's nose pointed directly at the terminal hovering point.)

For the vertical plane the Γ+E angle for all six trajectory types is plotted in Fig. 11. A significant downward change in Γ+E approaching the nadir occurs during the final 200 ft in range-to-go for the constant sink rate and straight line trajectories. This can also be easily viewed from the trajectory profile in Fig. 8.

Figure 12 shows the aircraft-to-ship angle E versus R for all three horizontal trajectories. For the horizontal plane the angle E for the

Constant approach bearing; full sideslip

Constant terminal glide path angle, γ

Constant gravitational acceleration, g

Ship's velocity, V_{ship}, generating wind-over-deck

Aircraft's true airspeed, $V_a = V$, and sway damping, $Y_v = f(V_a)$

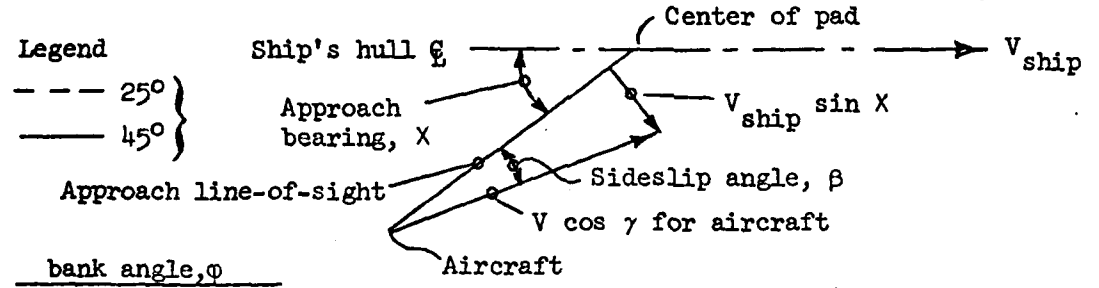

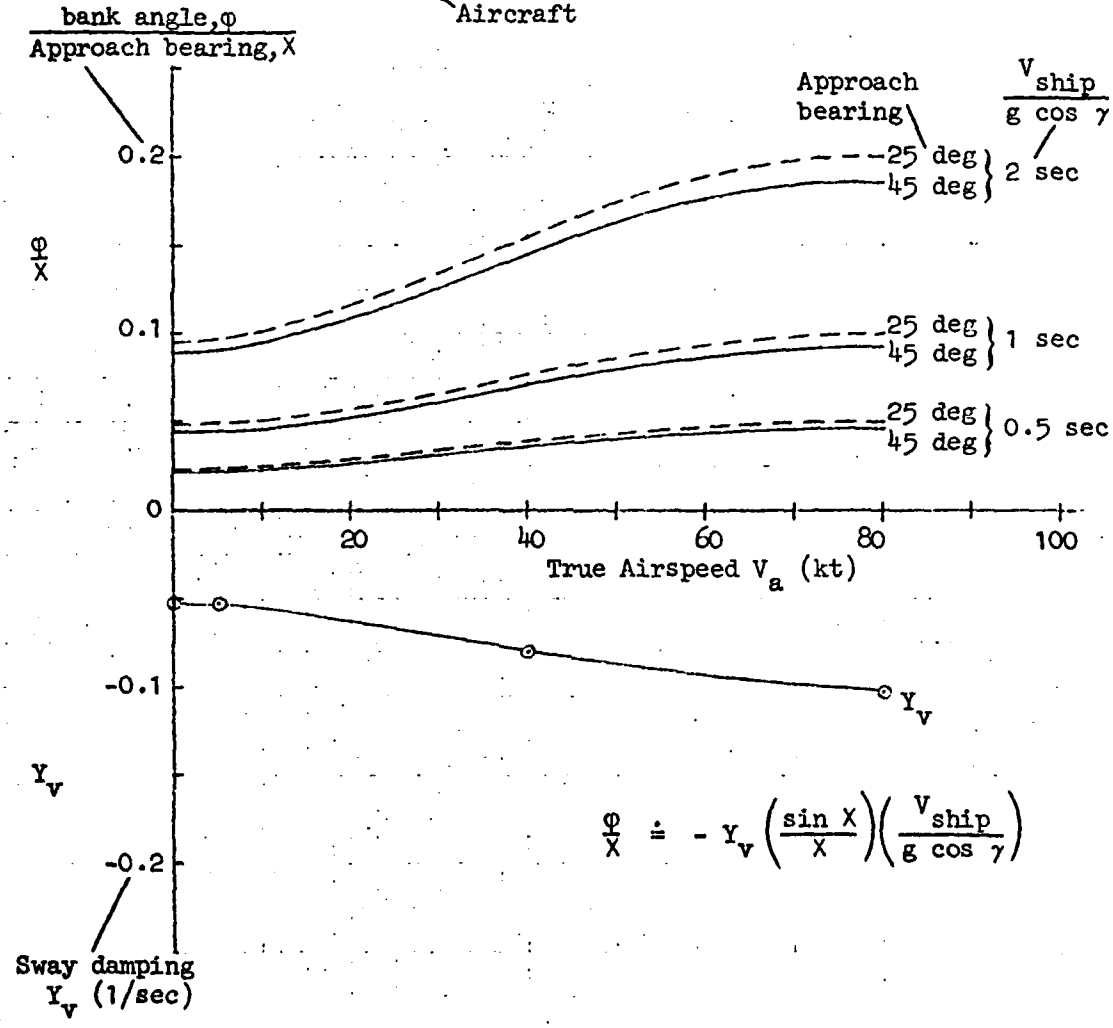

Figure 10. Relative Bank Angle Required for an Oblique Side Slipping Approach to a Moving Ship

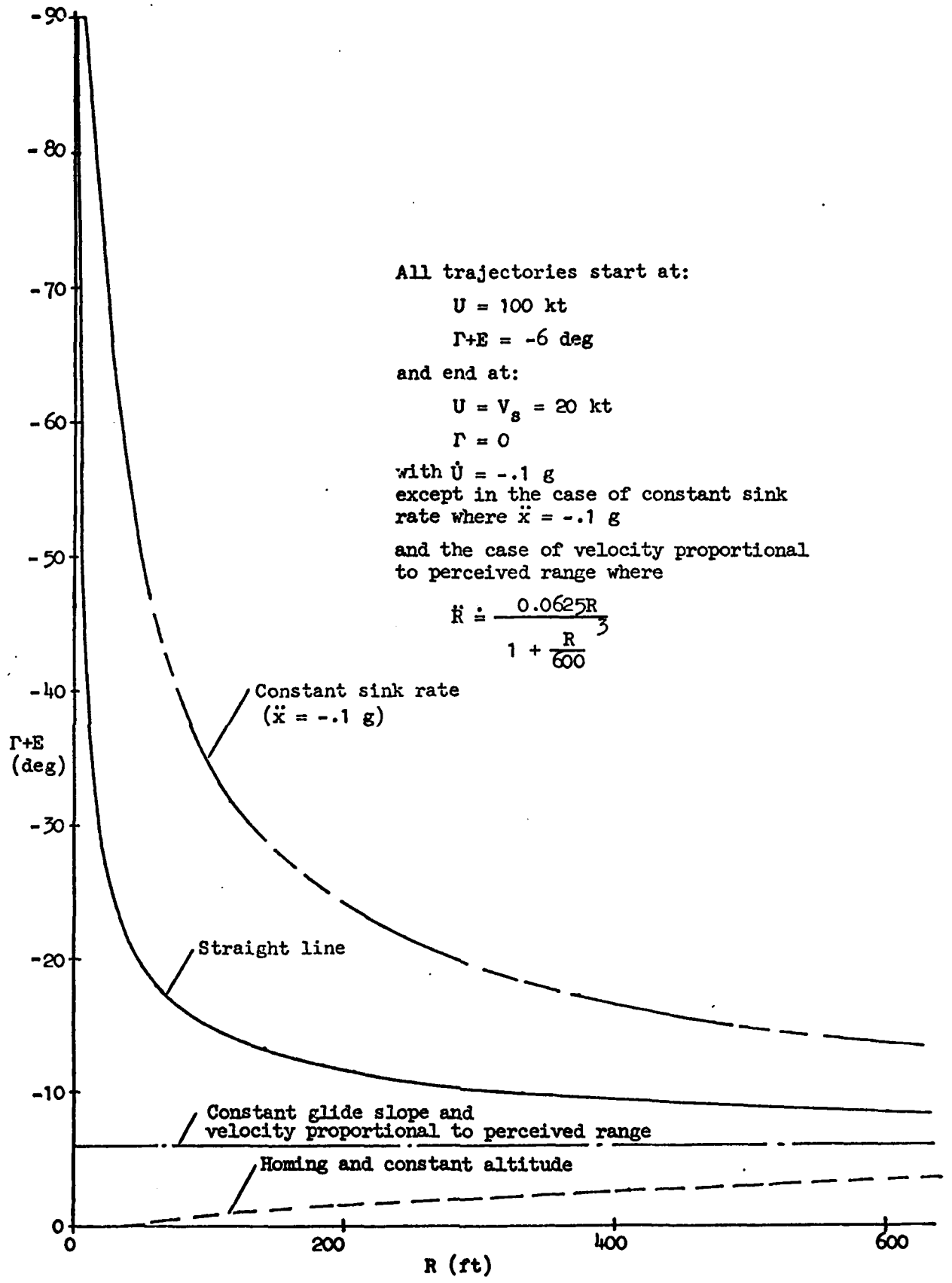

Figure 11. Relative Bearing from Ship Versus Range for Various Trajectory Types (Approach in Vertical Plane)

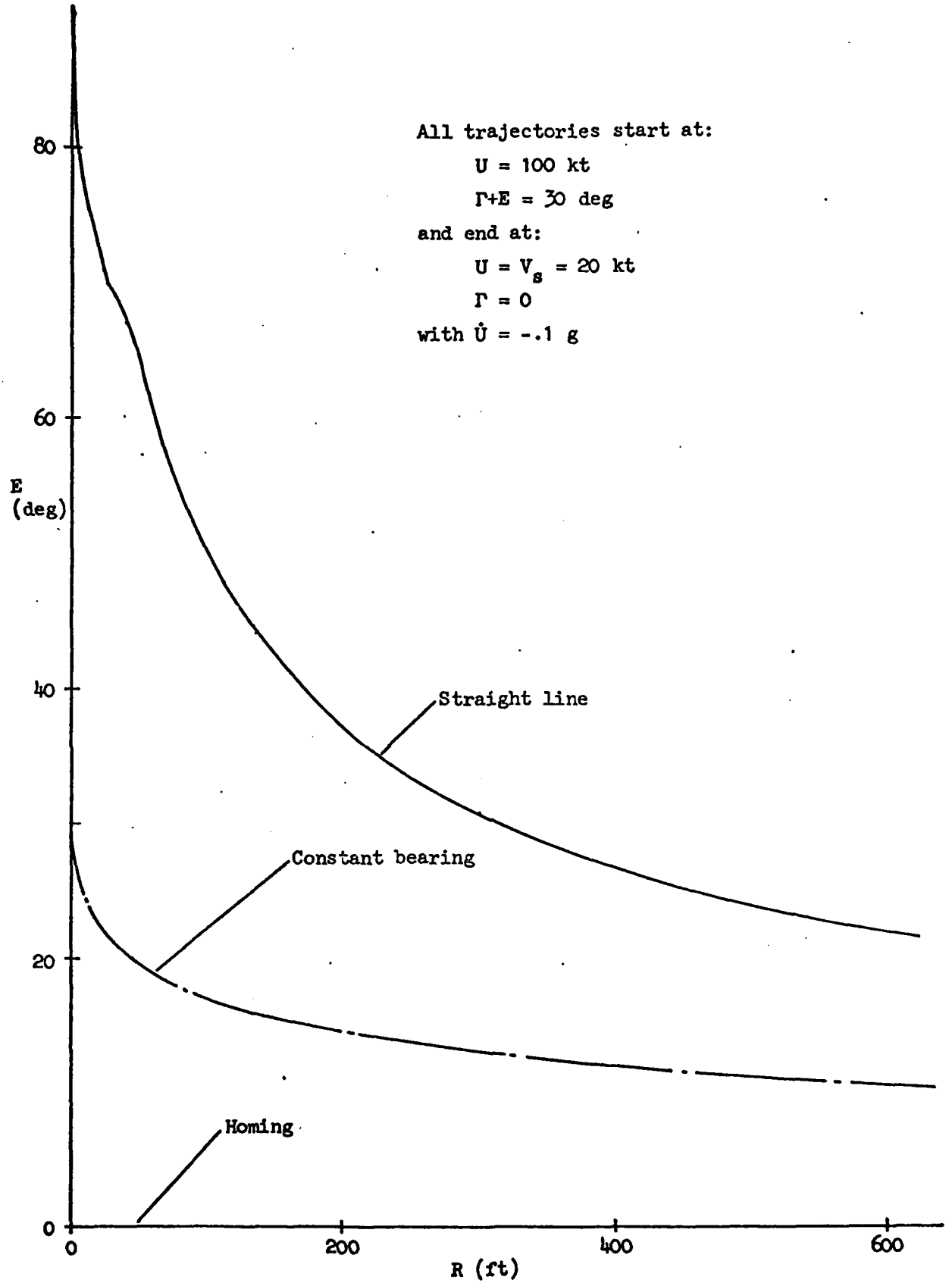

Figure 12. Aircraft-to-Ship Angle Versus Range (Horizontal Plane)

homing trajectory is identically zero by definition and for the straight line trajectory E approaches 90 deg as the range-to-go approaches zero.

From the aircraft-to-ship point of view the homing and constant altitude trajectories require the least field of view and the constant bearing nearly so. The straight line and constant sink rate trajectories require large changes in viewing angle at close range and therefore place inordinate requirements on field of view.

The material presented serves as a basis for the perspective views presented in Section III, where we shall consider the pilot's field-of-view requirements in more detail.

SECTION III

COMPARISON OF THE PILOT'S VIEW OF ESSENTIAL VISUAL ELEMENTS

This section illustrates and compares the aircraft pilot's view of the ship's landing pad and hangar face from several points throughout each nominal approach trajectory at constant deceleration described in Section II in the absence of disturbances*. Our objective is to project a three-dimensional object (pad and hangar) defined in a ship-based axis system onto a two-dimensional cartesian "picture plane" located at a distance, a, along a reference line of sight (LOS) called the optical axis (O-axis) in front of the pilot or observer in an aircraft-based body axis system. The cartesian projection algorithm used for illustrating the pilot's field of view in this picture plane is based on that recommended in Ref. 39 and differs from the spherical projection algorithm employed in Ref. 2. The mathematical details of the development of the projection algorithm used herein are given in Ref. 40.

The cartesian projection algorithm involves a tangent function of the subtended viewing angle and will yield a realistic picture of any three-dimensional object (albeit scaled) as long as the subtended viewing angle is small (i.e., less than 10 to 15 deg). The object will appear distorted for large values of the subtended viewing angle, because the tangent function becomes nonlinear. For example, it is impossible by Euclidian geometry to project an object that is in the observer's plane which is orthogonal to the optical axis (O-axis) onto another plane that is perpendicular to the O-axis and in front of the observer by distance a.

This limitation could be overcome, however, by placing the observer at the center of a sphere. The inside of the sphere could then be divided

---

* The pilot's view of the ship's pad from the velocity-proportional-to-perceived-range trajectory described in Section II will be nearly the same as that from the constant bearing trajectory.

into segments and approximated as flat surfaces. The drawback to this type of scheme, however, is the number of segments required to project a wide field of view. For example, the number of segments required to project the entire 360-deg visual field onto the inside of a sphere is:

$$N = \frac{4\pi}{\kappa^2} = 4\pi \frac{a}{\ell}$$

where a is the sphere radius, ℓ is the arc length of one segment (assume square segments), and $\kappa = \ell/a$. Thus two hundred 1.57 ft^2 segments would be required for a sphere with a 5 ft radius and $\kappa = 14.37$ deg!

A. EXAMPLES OF THE PILOT'S VIEW FROM EACH NOMINAL TRAJECTORY WITHOUT AIRCRAFT PERTURBATIONS

Field-of-view requirements based on the cartesian projection algorithm will be demonstrated for a V/STOL aircraft on final approach to a moving ship. Figure 13 defines the dimensions of a typical landing pad and hangar face aboard a destroyer of the USS Spruance Class (DD963 through DD966, according to Ref. 37 and p.420 of Ref. 38). The point M shown in Fig. 13 represents the target hover point. The seven points shown are used to represent the landing pad (i = 1, 2, 3, 4), hangar face (i = 1, 2, 6, 7), and drop line (i = 4, 5). The two squares shown in the forward right and left corners of the landing pad are both 10 ft by 10 ft. The 12 ft radius circle represents the target touchdown zone. The seven points, two squares, and the circle will be projected onto a viewing plane 10 cm in front of the observer (i.e., a = 10 cm). Thus the proper viewing angles will be preserved when the projection plane is held 10 cm in front of one eye. For all examples except that in Fig. 20 the reference line of sight (LOS) for the picture plane will be to the center of the landing pad. In Fig. 20 the reference LOS for the picture plane is shifted to the center of the upper edge of the hangar face.

Three types of approach trajectories will be considered first: "homing," "straight line" (in inertial space), and "constant bearing" (relative to the ship). In addition, a fourth "constant sink rate" trajectory and a

Location of Points to be Projected, P_i/S :

i	x_i/S	y_i/S	z_i/S
1	30 ft	20 ft	0 ft
2	30	−20	0
3	−30	−20	0
4	−30	20	0
5	−30	20	10
6	30	−20	−20
7	30	20	−20

Squares: 10 ft by 10 ft
Circle: 12 ft radius

0	0	0	0	(center of deck pad)
0'	30	0	-20	(center of upper edge of hangar face will become alternate origin for hovering projections)
3'	10	-20	0	
4'	10	20	0	

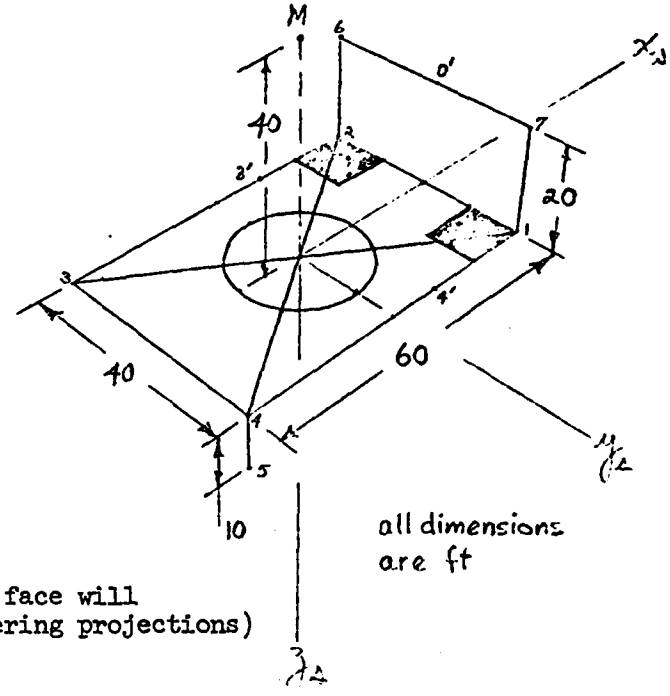

Figure 13. Dimensions of Landing Pad, Hangar Face, Drop Line, and Pad Markings

fifth "constant altitude" trajectory in the vertical plane will be combined with a constant bearing trajectory in the horizontal plane. Detailed descriptions of these trajectories can be found in Section II.

The results of the field of view calculations for the homing, straight line, constant bearing, and constant sink rate trajectories are presented in Figs. 14 through 18, respectively. The origin of the horizontal viewing angle (λ_i) axis corresponds to the horizontal reference line of sight relative to the nose of the aircraft at each value of slant range, R_m; thus the centers of the landing pads appear to be in the same horizontal line of sight for the homing and constant bearing trajectories, but not for the straight line trajectory. The origin of the vertical viewing angle (μ_i) axis corresponds to the vertical line of sight; thus the centers of the landing pads reflect the depressed elevation angles relative to the horizon at each slant range, R_m.

When viewing the perspective drawings shown in Figs. 14 through 18, it must be remembered that the abscissa and the ordinate of each view in the cartesian picture plane represent tangent functions of the viewing angles λ and μ. As long as the aircraft (pitch and roll) attitude is approximately level, field-of-view requirements for the nominal unperturbed approach trajectories may be interpreted directly in terms of the angles λ and μ-LOS_v for all trajectories except the straight line (in inertial space), for which the horizontal field-of-view requirement must be interpreted in terms of $\lambda + \Delta\psi$.

As mentioned previously, the correct viewing angles in Figs. 14 through 18 are preserved only when the perspective drawings are held 10 cm in front of one eye.

Figures 19 and 20 are projections of the landing pad and hangar face, respectively, when the aircraft has reached the hover point 40 ft over the center of the pad ($R_m \doteq 0$). The viewing distance for these two figures has been changed to 5 cm (i.e., a = 5 cm) for the purpose of reducing the size of the projections. Thus the correct angular relations in Figs. 19 and 20 are preserved only when the paper is held 5 cm in front of one eye.

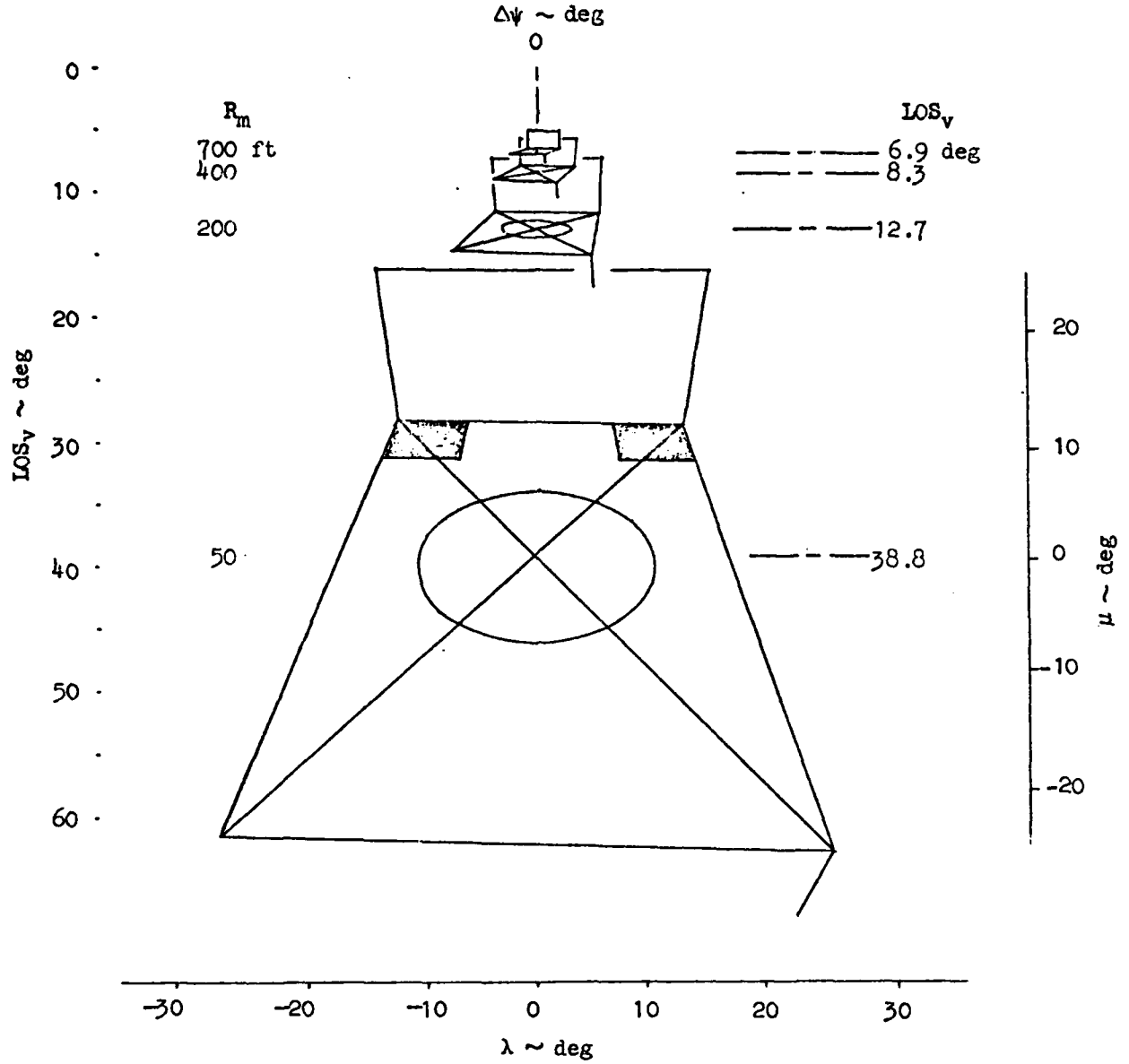

$\Delta\psi$ = Relative bearing angle of line of sight to center of landing pad with respect to aircraft nose. (This scale is not to be used in determining the subtended angle of any other point on the pad. $E = \Delta\psi$, if $\beta = 0$)

LOS_V = Depressed elevation angle of line of sight to center of landing pad. (This scale is not to be used in determining the subtended angle of any other point on the pad)

R_m = Observer's slant range to target hover point 40 ft above center of landing pad

λ, μ = Viewing angle (This scale may be used to determine the subtended vertical or horizontal angle of any point on the pad)

Figure 14. Perspective Views of Landing Pad for a Homing Trajectory (Viewing angles are preserved when page is held 10 cm in front of eye)

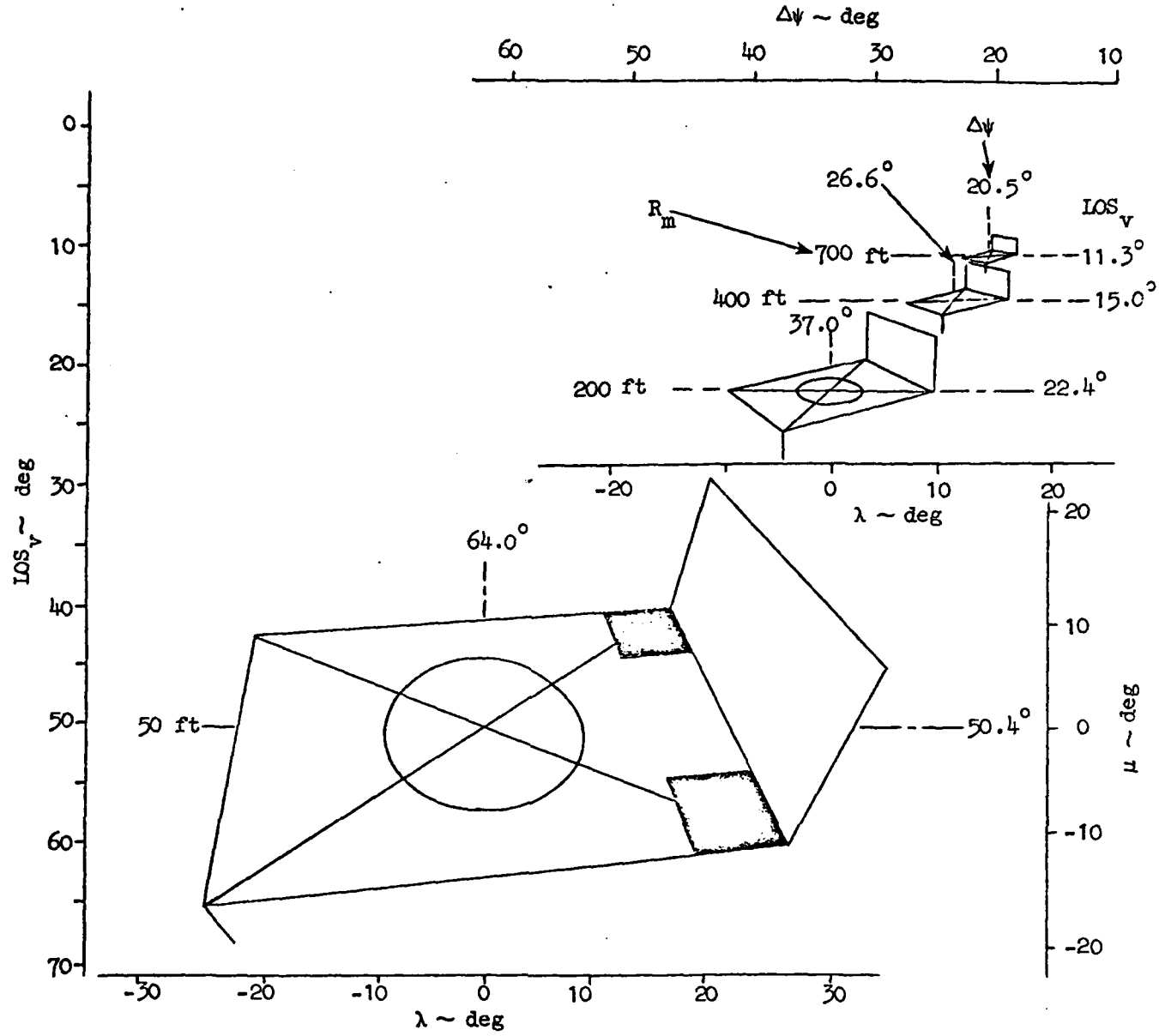

$\Delta\psi$ = Relative bearing angle of line of sight to center of landing pad with respect to aircraft nose. (This scale is not to be used in determining the subtended angle of any other point on the pad. E = $\Delta\psi$, if $\beta = 0$)

LOS_V = Depressed elevation angle of line of sight to center of landing pad. (This scale is not to be used in determining the subtended angle of any other point on the pad)

R_m = Observer's slant range to target hover point 40 ft above center of landing pad

λ, μ = Viewing angle (This scale may be used to determine the subtended vertical or horizontal angle of any point on the pad)

Figure 14. Perspective Views of Landing Pad for a Straight Line Trajectory (Viewing angles are preserved when page is held 10 cm in front of eye)

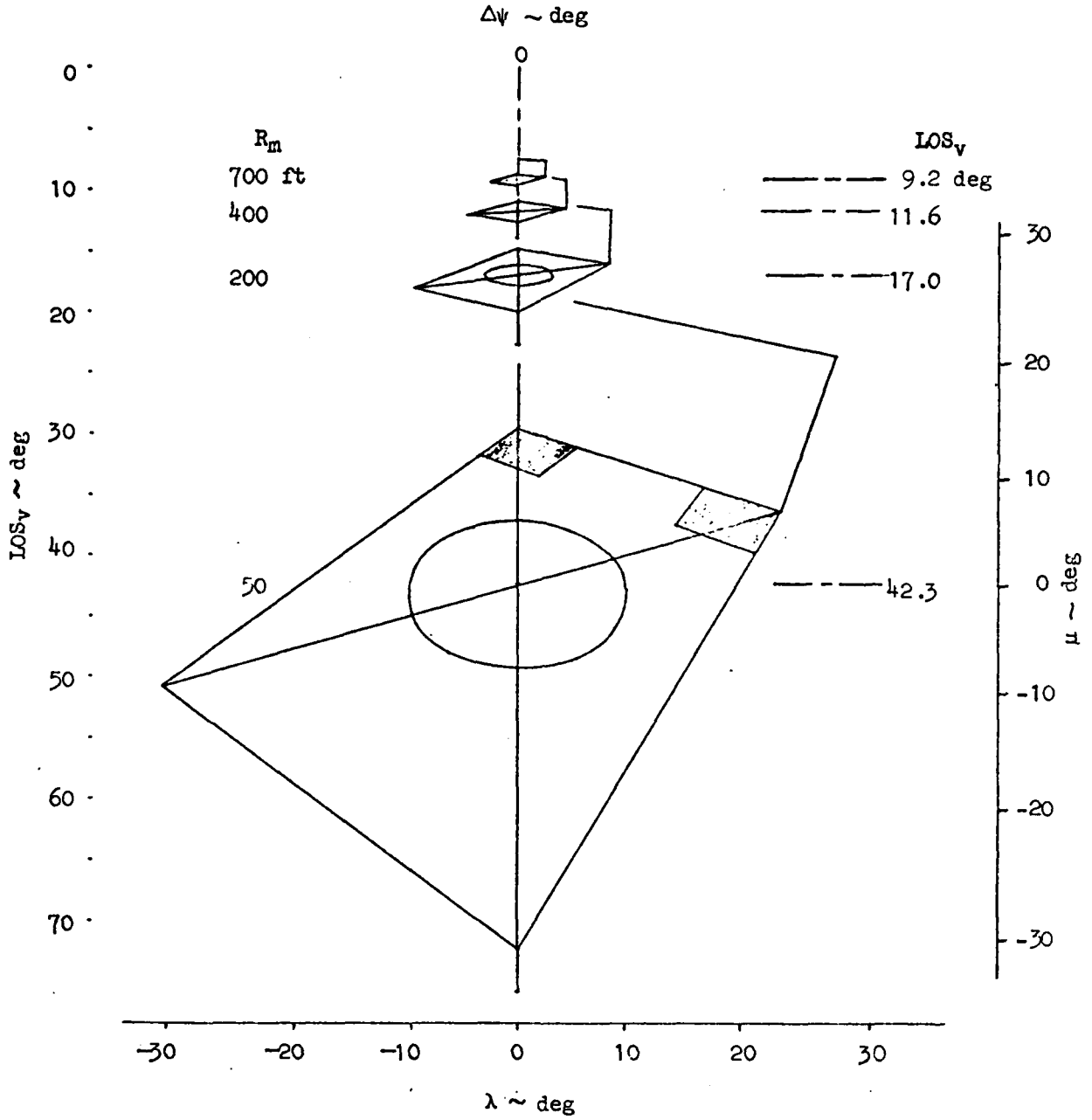

$\Delta\psi$ = Relative bearing angle of line of sight to center of landing pad with respect to aircraft nose. (This scale is not to be used in determining the subtended angle of any other point on the pad. $E = \Delta\psi$, if $\beta = 0$)

LOS_V = Depressed elevation angle of line of sight to center of landing pad. (This scale is not to be used in determining the subtended angle of any other point on the pad)

R_m = Observer's slant range to target hover point 40 ft above center of landing pad

λ, μ = Viewing angle (this scale may be used to determine the subtended vertical or horizontal angle of any point on the pad)

Figure 16. Perspective Views of Landing Pad for a Constant Bearing Trajectory (Viewing angles are preserved when page is held 10 cm in front of eye)

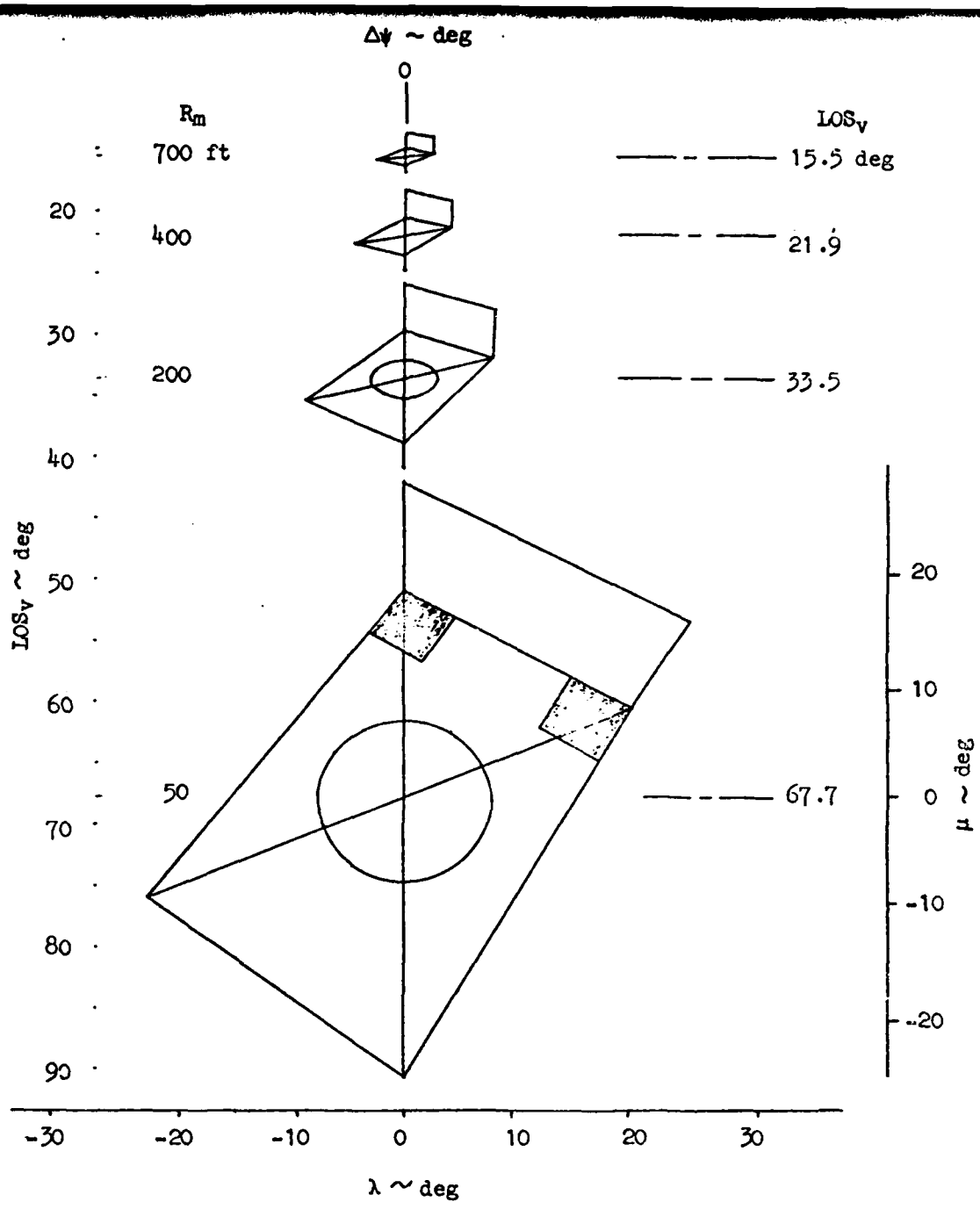

$\Delta\psi$ = Relative bearing angle of line of sight to center of landing pad with respect to aircraft nose. (This scale is not to be used in determining the subtended angle of any other point on the pad. $E = \Delta\psi$, if $\beta = 0$)

LOS_V = Depressed elevation angle of line of sight to center of landing pad. (This scale is not to be used in determining the subtended angle of any other point on the pad)

R_m = Observer's slant range to target hover point 40 ft above center of landing pad

λ, μ = Viewing angle (this scale may be used to determine the subtended vertical or horizontal angle of any point on the pad)

Figure 17. Perspective Views of Landing Pad for a Constant Sink Rate Trajectory at Constant Bearing (Viewing angles are preserved when page is held 10 cm in front of eye)

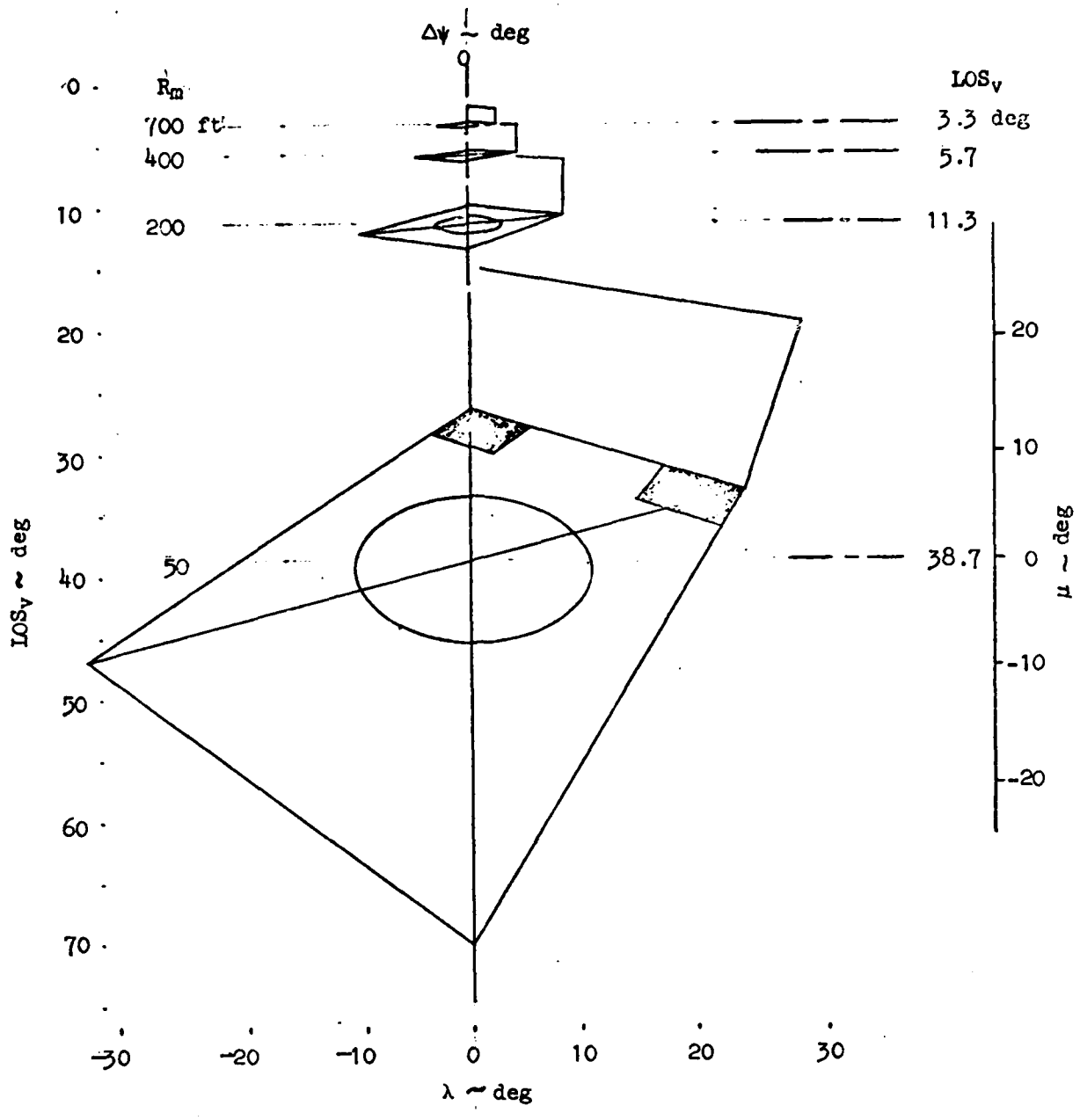

Δψ = Relative bearing angle of line of sight to center of landing pad with respect to aircraft nose. (This scale is not to be used in determining the subtended angle of any other point on the pad. E = Δψ, if β = 0)

LOS_V = Depressed elevation angle of line of sight to center of landing pad. (This scale is not to be used in determining the subtended angle of any other point on the pad)

R_m = Observer's slant range to target hover point 40 ft above center of landing pad

λ,μ = Viewing angle (This scale may be used to determine the subtended vertical or horizontal angle of any point on the pad)

Figure 18. Perspective Views of Landing Pad for a Constant Altitude Trajectory (Viewing angles are preserved when page is held 10 cm in front of eye)

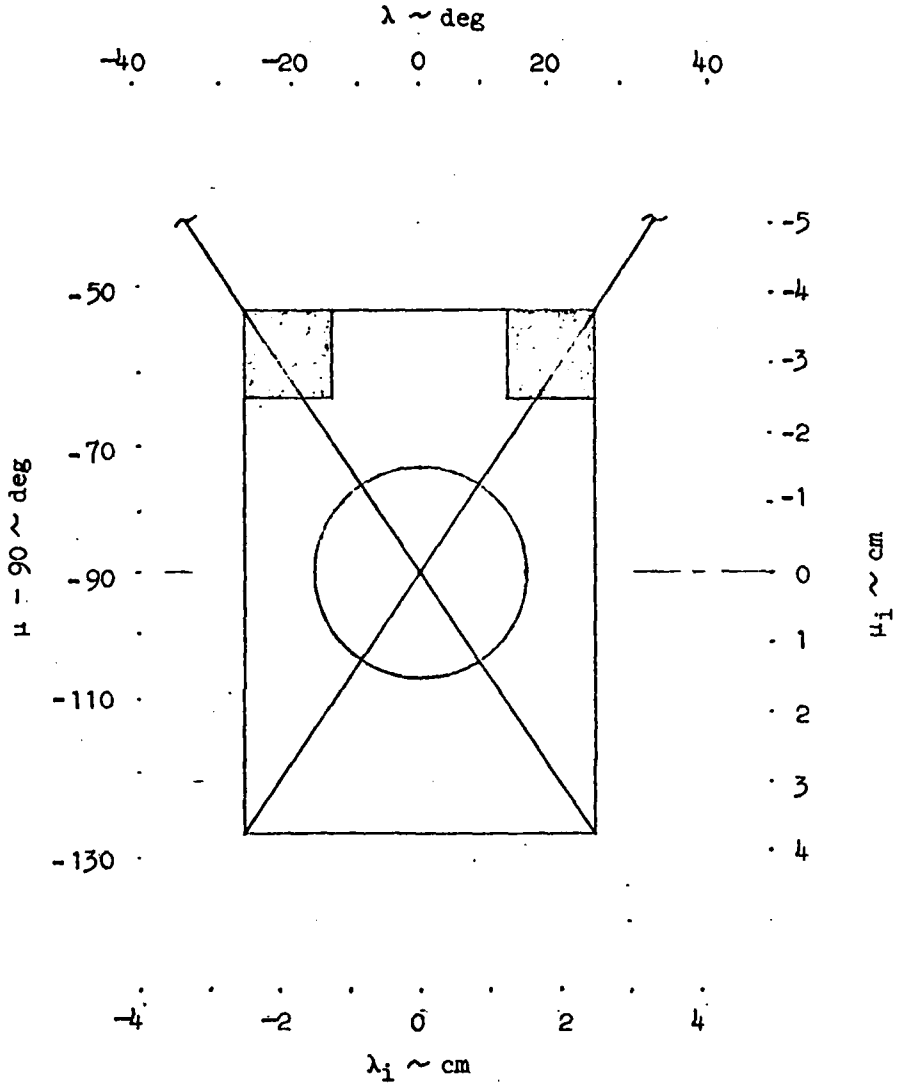

μ , λ = Vertical and Horizontal Viewing Angles, Respectively (These scales may be used to determine the subtended vertical or horizontal of any point on the pad)

λ_i = a tan λ

μ_i = a tan μ

a = 5 cm = Viewing Distance of Projection Plane in Front of Observer

Figure 19. Perspective View of Landing Pad for Aircraft 40 ft Above Landing Pad and Line of Sight Through Center of Pad (Viewing angles are preserved when page is held 5 cm in front of eye)

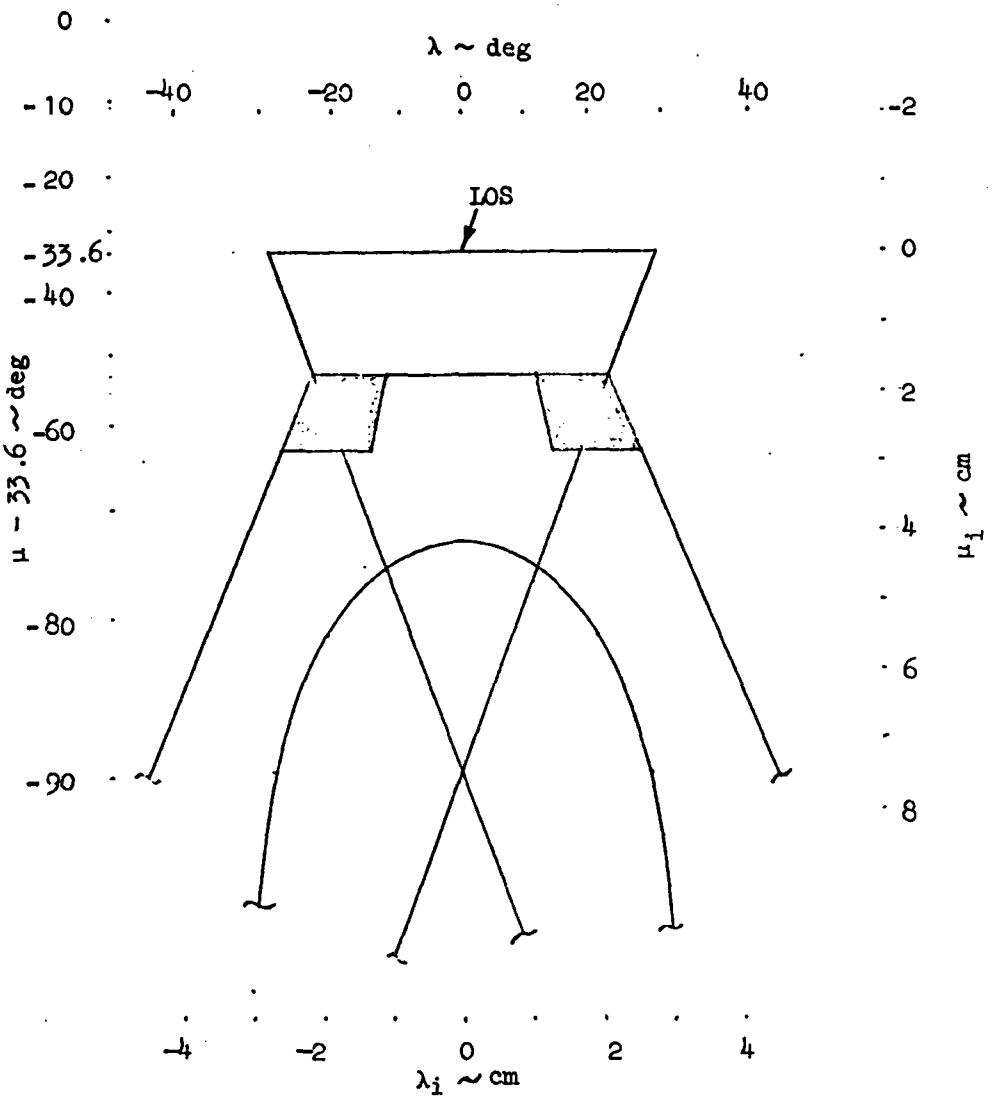

μ , λ = Vertical and Horizontal Viewing Angles, Respectively (These scales may be used to determine the subtended vertical or horizontal of any point on the pad)

λ_i = a tan λ

μ_i = a tan μ

a = 5 cm = Viewing Distance of Projection Plane in Front of Observer

Figure 20. Perspective View of Landing Pad for Aircraft 40 ft Above Landing Pad and Line of Sight Through Top and Center of Hangar Face (Viewing angles are preserved when page is held 5 cm in front of eye)

We have elected in Section IV to summarize some field-of-view requirements and tentative conclusions based on the foregoing examples of the pilot's view from each nominal trajectory without aircraft perturbations. In the next topic we shall illustrate the additional field-of-view requirements imposed by controlled aircraft perturbations caused by the relatively severe disturbance environment associated with sea state 5 and 43 kt wind-over-deck.

B. EXAMPLES OF THE PILOT'S VIEW FROM 50 FT RANGE TO THE HOVERING POINT WITH CONTROLLED AIRCRAFT PERTURBATIONS

The field of view (FOV) from the aircraft cockpit required to see a point of regard on the recovery area during an approach to hovering over the area is a function of (a) the location of the point of regard itself on the ship, (b) the aircraft orientation, and (c) the relative position of the aircraft with respect to the ship, but the FOV may be restricted by cockpit occlusions. In the previous topic we have illustrated how the location of the point of regard on the ship and how the relative position of the undisturbed aircraft with respect to the ship affect the pilot's field of view. We have seen that the field-of-view requirements will be greatest near the ship in hovering and near-hovering flight. In this topic we wish to illustrate the combined effects of rotational and translational disturbances in the controlled aircraft motion on the hovering and near-hovering field-of-view requirements.

The details of the extensive analyses required to provide the examples shown in this topic are documented in Refs. 33 and 41 and will not be repeated here.* The results depend in a critical way on the predicted model of the ship's airwake disturbance environment adopted in Ref. 33 for sea state 5 and 43 kt wind-over-deck, which present quite a severe disturbance environment. Two examples of perturbed field-of-view requirements will be presented: (1) from 50 ft range-to-go (to the hovering point) on

---

* A method for introducing cockpit occlusions into the field-of-view analysis is also presented in Ref. 41.

a constant relative bearing trajectory and (2) from the hovering point itself 40 ft above the center of the landing pad.

Perturbations in the pilot's perspective view of the landing pad and hangar face used in this study (Fig. 13) can be represented by computing a linear sensitivity matrix of influence coefficients (or partial derivatives) for each point of regard with respect to each aircraft degree of freedom (i.e., three independent rotations and three orthogonal translations). An HP-67/97 computer program described in Ref. 41 was used to make these linear sensitivity calculations for the two examples to be shown here. The resulting arrays of influence coefficients for all points of regard used on the landing pad and hangar face are summarized in Tables 4 and 5 for 50-ft range and zero range-to-go, respectively. (The points i = 1, 2, etc., listed in Tables 4 and 5 are defined in the nominal perspective views shown in Figs. 13 and 21).

By expanding the lateral and vertical viewing angles of each point of regard in the picture plane in a Taylor's series truncated to include only the linear term, we can use the partial derivatives listed in Tables 4 and 5 to represent linear perturbations in the pilot's perspective view of the landing pad and hangar face as the aircraft translates relative to the ship.

In order to express perturbations in the pilot's field of view with respect to an aircraft reference axis, we shall employ the two coordinates FOV_{λ_i} and FOV_{μ_i}. FOV_{λ_i} and FOV_{μ_i} are entirely consistent with picture plane coordinates λ_i and μ_i, except that the origin of FOV_{λ_i}, FOV_{μ_i} in the picture plane is where the aircraft longitudinal body reference axis intercepts the picture plane. (In contradistinction the origin of λ_i, μ_i is where the optical axis or LOS to the boresight point intercepts the picture plane.) Linear perturbations in FOV_{λ_i}, FOV_{μ_i} are derived in Ref. 41 and expressed in the form:

TABLE 4

SUMMARY OF PERSPECTIVE PERTURBATION MATRICES FOR R_m = 50 FT

i	z_i (ft)	$A_i(0)$ (ft)	$\lambda_i(0)$ (cm)	$\mu_i(0)$ (cm)	$\frac{\partial\lambda_i}{\partial x_B}$ (cm/ft)	$\frac{\partial\lambda_i}{\partial y_B}$ (cm/ft)	$\frac{\partial\lambda_i}{\partial z_B}$ (cm/ft)	$\frac{\partial\mu_i}{\partial x_B}$ (cm/ft)	$\frac{\partial\mu_i}{\partial y_B}$ (cm/ft)	$\frac{\partial\mu_i}{\partial z_B}$ (cm/ft)
1	0.0	77.5	4.30	-1.20	0.0462	0.0634	0.0317	-0.0262	0.0505	0.0058
2	0.0	93.9	0.0	-2.55	0.0	0.0762	0.0	-0.0551	0.0	0.0202
3	0.0	57.0	-5.85	1.65	-0.0662	0.0016	-0.0797	0.0366	-0.0936	0.0028
4	0.0	40.5	0.0	6.00	0.0	-0.1794	0.0	0.140	0.0	0.0668
5	10.0	47.3	0.0	6.70	0.0	-0.1535	0.0	0.102	0.0	0.0984
6	-20.0	80.4	0.0	-4.85	0.0	0.0900	0.0	-0.0846	0.0	0.0034
7	-20.0	64.0	5.2	-3.75	0.0796	0.0832	0.0332	-0.0524	0.0414	-0.0295

a = 10 cm $\qquad \gamma'_{v_o}$ = 42.3 deg $\qquad r_o$ = 67.2 ft

N.B. In this table the origin in ship coordinates $(x_i, y_i, z_i)_s$ for the location of points (i) to be projected in the picture plane is at the center of the deck pad in Fig. 13.

TABLE 5

SUMMARY OF PERSPECTIVE PERTURBATION MATRICES FOR R_m = 0 FT

i	z_i (ft)	$A_i(0)$ (ft)	$\lambda_i(0)$ (cm)	$\mu_i(0)$ (cm)	$\frac{\partial\lambda_i}{\partial x_B}$ (cm/ft)	$\frac{\partial\lambda_i}{\partial y_B}$ (cm/ft)	$\frac{\partial\lambda_i}{\partial z_B}$ (cm/ft)	$\frac{\partial\mu_i}{\partial x_B}$ (cm/ft)	$\frac{\partial\mu_i}{\partial y_B}$ (cm/ft)	$\frac{\partial\mu_i}{\partial z_B}$ (cm/ft)
1	20.	47.2	2.12	1.76	0.0260	0.0252	0.0421	0.0035	0.0597	0.0621
2	20.	47.2	-2.12	1.76	-0.0260	0.0252	-0.0421	0.0035	-0.0597	0.0621
6	0.	36.1	-2.77	0.	-0.0639	0.0425	-0.0425	0.0	-0.0510	0.0
7	0.	36.1	2.77	0.	0.0639	0.0425	0.0425	0.0	0.0510	0.0
11	20.	47.2	1.06	1.76	0.0130	0.0065	0.0210	0.0035	0.0298	0.0621
12	20.	47.2	-1.06	1.76	-0.0130	0.0065	-0.0210	0.0035	-0.0298	0.0621
13	20.	38.9	-2.57	2.85	-0.0326	-0.0060	-0.0740	0.0306	-0.0879	0.0863
14	20.	38.9	-1.29	2.85	-0.0163	-0.0334	-0.0353	0.0306	-0.0441	0.0863
15	20.	38.9	1.29	2.85	0.0163	-0.0334	0.0353	0.0306	0.0441	0.0863
16	20.	38.9	2.57	2.85	0.0326	0.0060	0.0740	0.0306	0.0879	0.0863
0	20.	22.2	0.	7.48	0.0	-0.2240	0.0	0.1571	0.0	0.3724
3'	20.	30.55	-3.27	4.53	-0.0437	-0.0492	-0.1276	0.0745	-0.1422	0.1558
4'	20.	30.55	3.27	4.53	0.0437	-0.0492	0.1276	0.0745	0.1422	0.1558

a = 5 cm $\qquad \gamma'_{v_o}$ = 33.6 deg $\qquad r_o$ = 36.1 ft

N.B. In this table the origin in ship coordinates for the location of points (i) to be projected in the picture plane in Fig. 21 is at the center of the upper edge of the hangar face in Fig. 13.

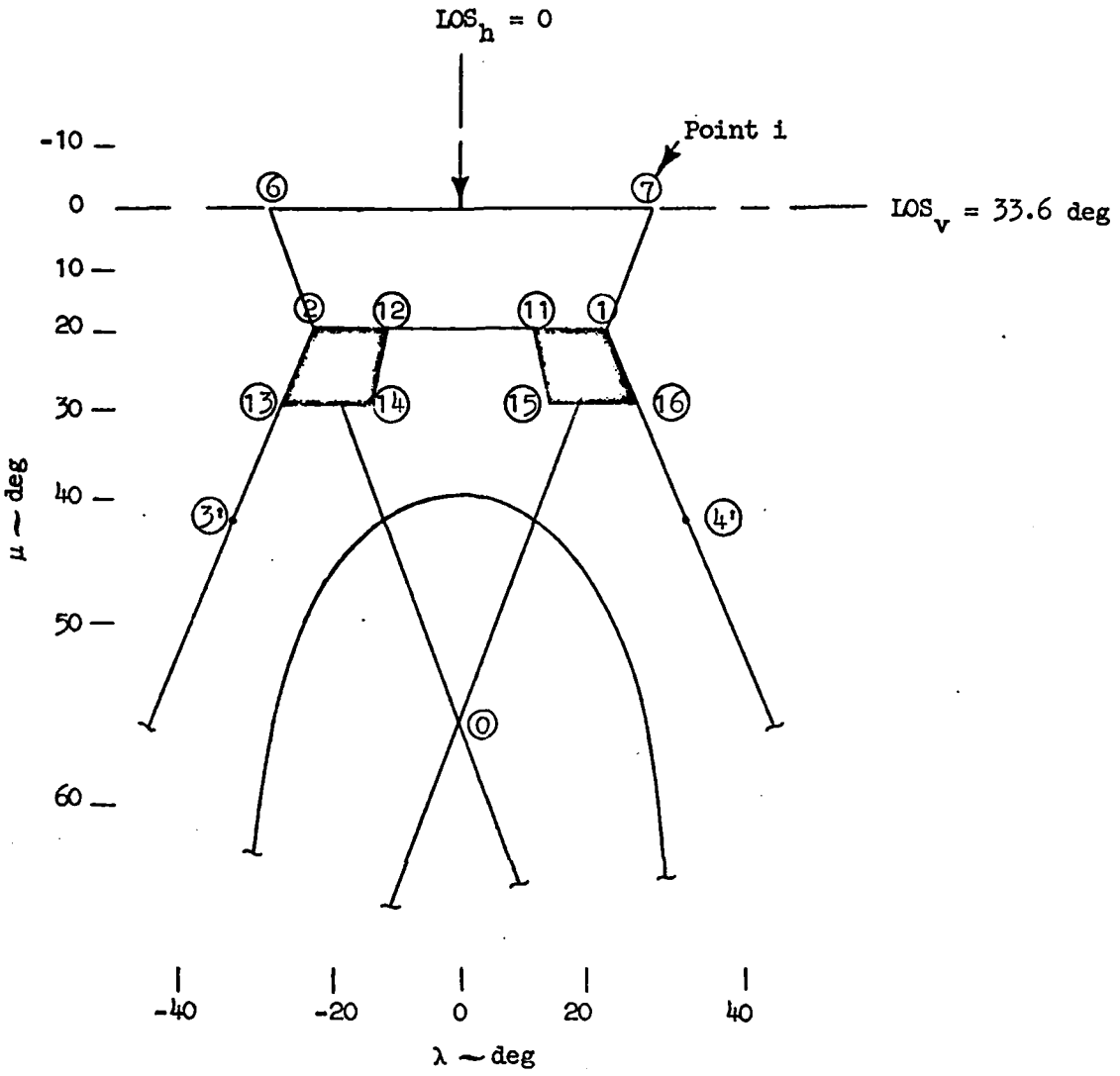

LOS$_h$ = Bearing angle of line of sight to top center of hangar door

LOS$_v$ = Depressed elevation angle of line of sight to top center of hangar door

R_m = Observer's slant range to target hover point 40 ft above center of landing pad (zero in this case)

μ, λ = Viewing angle (this scale may be used to determine the subtended vertical or horizontal angle of any point on the pad)

Figure 21. Numerical Identification of Points of Regard in the Perspective View of Landing Pad for Aircraft 40 ft Above Landing Pad and Line of Sight Through Top and Center of Hangar Face (Viewing angles are preserved when page is held 5 cm in front of eye)

$$\underbrace{\begin{Bmatrix} \epsilon_{FOV_{\lambda_i}} \\ \epsilon_{FOV_{\mu_i}} \end{Bmatrix}}_{\text{Linear perturbations in the pilot's FOV in the picture plane}} = \underbrace{\begin{bmatrix} F_R \end{bmatrix} \begin{Bmatrix} \psi \\ \theta \\ \varphi \end{Bmatrix}}_{\text{Rotational perturbations at the LOS in the picture plane}} + \underbrace{\begin{bmatrix} F_T \end{bmatrix} \begin{Bmatrix} x_B \\ y_B \\ z_B \end{Bmatrix}}_{\text{Translational perturbations at the LOS in the picture plane}} + \underbrace{\begin{bmatrix} S_{P_i} \end{bmatrix} \begin{Bmatrix} x_B \\ y_B \\ z_B \end{Bmatrix}}_{\text{Translational perturbations in perspective at points of regard other than the LOS in the picture plane}} \quad (1)$$

in terms of perturbed aircraft rotational orientation variables ψ, θ, φ and perturbed aircraft translational position variables x_B, y_B, z_B.

If the initial aircraft heading is aligned with the LOS to the ship, initial pitch attitude is zero, and wings are initially level, the matrices in Eq. 1 reduce to

$$\begin{bmatrix} F_R \end{bmatrix} = \begin{bmatrix} -1 & 0 & 0 \\ 0 & \sec^2 \gamma'_{V_O} & 0 \end{bmatrix}$$

$$\begin{bmatrix} F_T \end{bmatrix} = \begin{bmatrix} 0 & \dfrac{-a \sec \gamma'_{V_O}}{r_o} & 0 \\ \dfrac{a \tan \gamma'_{V_O}}{r_o \cos \gamma'_{V_O}} & 0 & \dfrac{-a \sec \gamma'_{V_O}}{r} \end{bmatrix}$$

$$\begin{bmatrix} S_{P_i} \end{bmatrix} = \begin{bmatrix} \dfrac{\partial \lambda_i}{\partial x_B} & \dfrac{\partial \lambda_i}{\partial y_B} & \dfrac{\partial \lambda_i}{\partial z_B} \\ \dfrac{\partial \mu_i}{\partial x_B} & \dfrac{\partial \mu_i}{\partial y_B} & \dfrac{\partial \mu_i}{\partial z_B} \end{bmatrix}$$

where a = pilot's eye-to picture plane distance

r_o = initial range to the boresight point

γ'_{V_O} = initial LOS depression angle with respect to the horizon

and the partial derivatives in $\begin{bmatrix} S_{P_i} \end{bmatrix}$ are given in Tables 4 and 5.

Within regions of the field of view where the linear relationships (Eq. 1) provide a sufficiently valid representation of changes in perspective, the appropriate influence coefficients in Tables 4 and 5 for selected visual points of regard by the pilot can be used to estimate Gaussian statistical variances in the cartesian picture plane coordinates caused by the variances in the six aircraft degrees of freedom estimated in Ref. 33. Corresponding distributions of perturbations in terms of viewing angles will, however, tend to be increasingly skewed as the point of regard (i) departs from the boresight or optical axis of the picture plane because of the tangent relationship between picture plane coordinates and viewing angles. Nevertheless we can approximate the (non-Gaussian) angular variances in the field of view in terms of the (Gaussian) variances in the picture plane coordinates in order to provide a measure of the additional field-of-view requirements imposed by the disturbance environment on the aircraft.

The picture plane coordinate variances $\sigma^2_{\epsilon_{FOV_{\lambda_i}}}$ and $\sigma^2_{\epsilon_{FOV_{\mu_i}}}$ can be expressed in terms of the aircraft motion error variances σ^2_ψ, σ^2_θ, σ^2_φ, $\sigma^2_{x_B}$, $\sigma^2_{y_B}$, and $\sigma^2_{z_B}$ listed in Table 6 by forming expectations of squared values from Eq. 1 and recognizing the approximate statistical independence among the six aircraft degrees of freedom with an augmented control system which decouples x_B from θ, y_B from φ, and ψ from z_B in hovering.*

The picture plane coordinate variances so estimated are listed in Table 7 for the field of view from a 50 ft range to the target hover point and in Table 8 for the field of view from the target hover point 40 ft above the center of the landing pad. Each (i^{th}) point of regard on the pad and hangar face is identified numerically in correspondence with Figs. 22 and 23. The pilot's eye-to-picture plane distance is a, which is 10 cm in Table 7 and Fig. 22 and 5 cm in Table 8 and Fig. 23.

The lateral angular variance of each point of regard caused by the disturbance environment is approximated by one-half of the angular difference

---

* The customary covariances between x_B and θ, y_B and φ, and (for helicopters) ψ and z_B in hovering can be included by combining Eq. 1 with the perturbed motion equations for the airframe (e.g., Ref. 33) before forming the expectations of squared values from Eq. 1. This is, however, beyond the scope of the present work.

TABLE 6

SUMMARY OF ILLUSTRATIVE MOTION ERROR VARIANCES
FOR USE IN EXAMINING HOVERING FIELD-OF-VIEW REQUIREMENTS
(From Ref. 33)

Sea State 5

Wind-Over-Deck = 43 kt

Ship Speed, V_s = 25 kt

Clockwise Wave Direction Relative to Ship's Stern, μ = 120 deg

Mean-Squared Ship Motions at the Center of the Landing Pad (Relative to Inertial Space) for the DD963

Ship Motion		Variance
Roll	σ_φ^2	$(2.02 \text{ deg})^2$
Pitch	σ_θ^2	$(0.77 \text{ deg})^2$
Yaw	σ_ψ^2	$(0.30 \text{ deg})^2$
Surge	σ_x^2	$(0.40 \text{ ft})^2$
Sway	σ_y^2	$(2.05 \text{ ft})^2$
Heave	σ_z^2	$(2.71 \text{ ft})^2$

Mean-Square Aircraft Motion Relative to Ship while Stationkeeping under Manual Control

Aircraft Motion		Variance
Roll	σ_φ^2	$(2.5 \text{ deg})^2$
Pitch	σ_θ^2	$(3.0 \text{ deg})^2$
Yaw	σ_ψ^2	$(2.1 \text{ deg})^2$
Surge	σ_x^2	$(11.6 \text{ ft})^2$
Sway	σ_y^2	$(15.5 \text{ ft})^2$
Heave	σ_z^2	$(19.5 \text{ ft})^2$

between the picture plane coordinates for each point of regard plus and minus one standard deviation in Tables 7 and 8. The required arctangent relationships are shown in the caption of each table and the angular variances so computed are listed to the right of the variances in picture plane coordinates (cm). Also listed in Tables 7 and 8 are the ratios of the (picture plane coordinate) variance for each (i^{th}) point of regard to the (corresponding) variance for the boresight point (i = 0). These ratios provide a convenient measure of the relative variability in each point of regard caused by the disturbance environment.

Only for the boresight point (i = 0) in Figs. 22 and 23 have we plotted the variability ellipse for one standard deviation in order to avoid the confused presentation resulting from overlapping ellipses about each of the points of regard. Nevertheless the rather large vertical field of view

TABLE 7

SUMMARY OF FIELD OF VIEW VARIANCES IN THE PICTURE PLANE FOR RANGE TO THE TARGET HOVER POINT, R_m = 50 ft

The pilot's eye-to-picture plane distance a = 5 cm. The lateral angular variance is approximated by

$$\left\{\frac{1}{2}\left|\arctan\left[(\lambda_i + \sigma_{\epsilon_{FOV_{\lambda_i}}})/a\right] - \arctan\left[(\lambda_i - \sigma_{\epsilon_{FOV_{\lambda_i}}})/a\right]\right|\right\}^2$$

and the vertical angular variance, by

$$\left\{\frac{1}{2}\left|\arctan\left[(\mu_i + \sigma_{\epsilon_{FOV_{\mu_i}}})/a\right] - \arctan\left[(\mu_i - \sigma_{\epsilon_{FOV_{\mu_i}}})/a\right]\right|\right\}^2$$

Refer to Fig. 22 for identification of each point of regard (λ_i, μ_i)

POINT OF REGARD i	LATERAL VARIANCE $\sigma^2_{\epsilon_{FOV_{\lambda_i}}}$		RELATIVE LATERAL STANDARD DEVIATION $\sigma^{(cm)}_{\epsilon_{FOV_{\lambda_i}}} / \sigma^{(cm)}_{\epsilon_{FOV_{\lambda_i}}}$	VERTICAL VARIANCE $\sigma^2_{\epsilon_{FOV_{\mu_i}}}$		RELATIVE VERTICAL STANDARD DEVIATION $\sigma^{(cm)}_{\epsilon_{FOV_{\mu_i}}} / \sigma^{(cm)}_{\epsilon_{FOV_{\mu_i}}}$
	$(cm)^2$	$(deg)^2$		$(cm)^2$	$(deg)^2$	
0	$(3.14)^2$	$(17.4)^2$	1.00	$(4.56)^2$	$(24.5)^2$	1.00
1	$(2.31)^2$	$(11.1)^2$	0.74	$(4.40)^2$	$(23.5)^2$	0.96
2	$(1.97)^2$	$(11.4)^2$	0.63	$(3.94)^2$	$(20.5)^2$	0.86
3	$(3.56)^2$	$(15.2)^2$	1.14	$(4.94)^2$	$(25.8)^2$	1.08
4	$(5.91)^2$	$(30.6)^2$	1.89	$(4.67)^2$	$(19.6)^2$	1.02
5	$(5.51)^2$	$(28.8)^2$	1.76	$(3.98)^2$	$(15.8)^2$	0.87
6	$(1.76)^2$	$(10.0)^2$	0.56	$(4.13)^2$	$(19.0)^2$	0.81
7	$(2.18)^2$	$(9.8)^2$	0.70	$(4.88)^2$	$(23.6)^2$	1.07

N.B. Only $(0.37\ cm)^2$ $(2.1\ deg)^2$ of lateral variance and only $(0.96\ cm)^2_{all\ i}$ $(5.5\ deg)^2_{i=0}$ of vertical variance are caused by the combined variances in aircraft orientation angles (σ^2_ψ, σ^2_θ, σ^2_φ) from Table 6. Balances of variance in viewing angles are caused by variances in components of aircraft translation ($\sigma^2_{x_B}$, $\sigma^2_{y_B}$, $\sigma^2_{z_B}$) from Table 6.

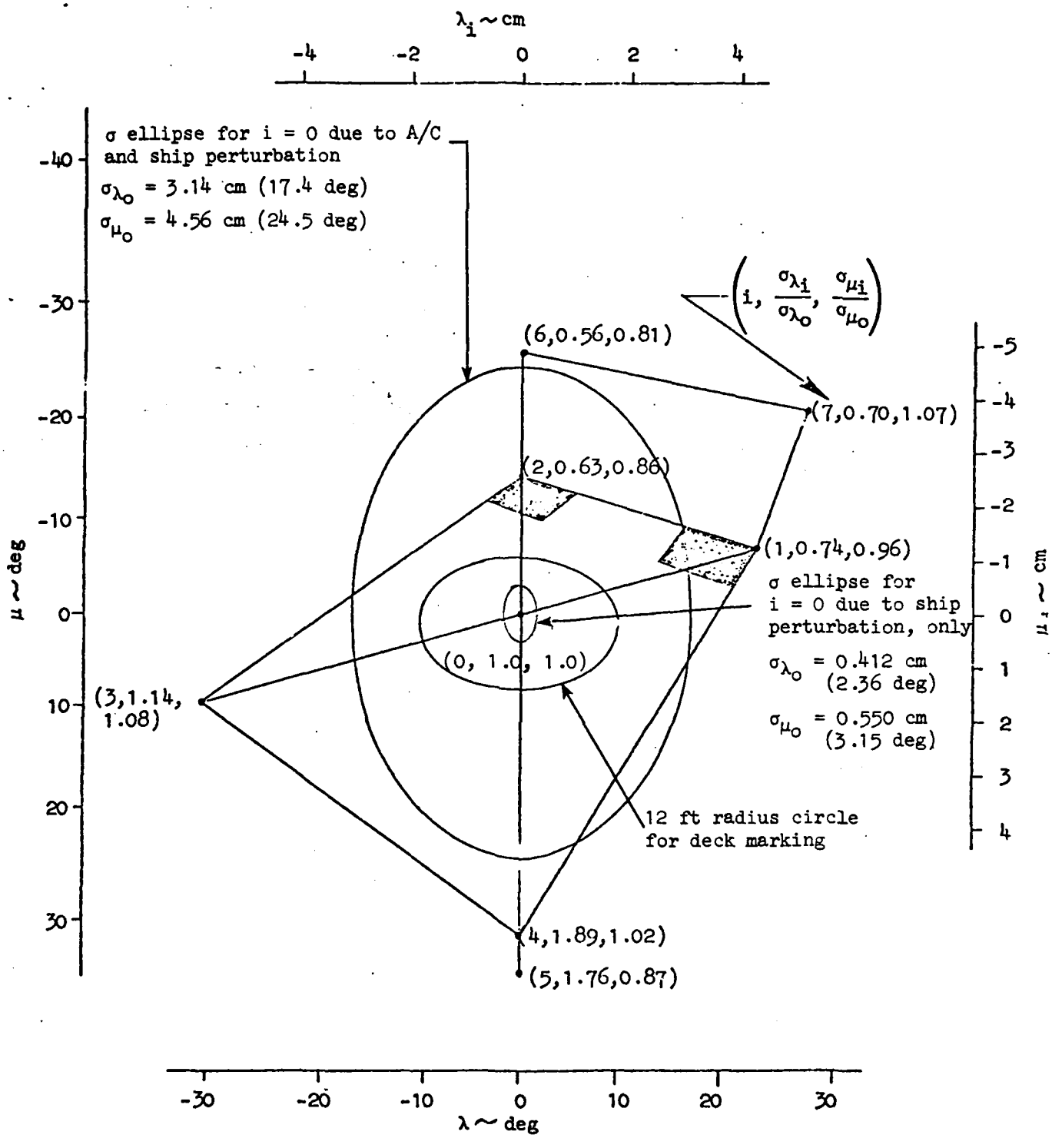

λ,μ = Viewing angle (This scale may be used to determine the subtended vertical or horizontal angle of any point on the pad)

Figure 22. Graphical Representation of σ Variation in Field of View for the R_m = 50 ft Case. (Viewing angles are preserved when page is held 10 cm in front of eye)

TABLE 8

SUMMARY OF FIELD OF VIEW VARIANCES IN THE PICTURE PLANE FOR RANGE TO THE TARGET HOVER POINT, R_m = 0 ft

The pilot's eye-to-picture plane distance a = 5 cm. The lateral angular variance is approximated by

$$\left\{\frac{1}{2}\left|\arctan\left[(\lambda_i + \sigma_{\epsilon_{FOV_{\lambda_i}}})/a\right] - \arctan\left[(\lambda_i - \sigma_{\epsilon_{FOV_{\lambda_i}}})/a\right]\right|\right\}^2$$

and the vertical angular variance, by

$$\left\{\frac{1}{2}\left|\arctan\left[(\mu_i + \sigma_{\epsilon_{FOV_{\mu_i}}})/a\right] - \arctan\left[(\mu_i - \sigma_{\epsilon_{FOV_{\mu_i}}})/a\right]\right|\right\}^2$$

Refer to Fig. 23 for identification of each point of regard (λ_i, μ_i)

POINT OF REGARD	LATERAL VARIANCE $\sigma^2_{\epsilon_{FOV_{\lambda_i}}}$		RELATIVE LATERAL STANDARD DEVIATION $\sigma^{(cm)}_{\epsilon_{FOV_{\lambda_i}}} / \sigma^{(cm)}_{\epsilon_{FOV_{\lambda_i}}}$	VERTICAL VARIANCE $\sigma^2_{\epsilon_{FOV_{\mu_i}}}$		RELATIVE VERTICAL STANDARD DEVIATION $\sigma^{(cm)}_{\epsilon_{FOV_{\mu_i}}} / \sigma^{(cm)}_{\epsilon_{FOV_{\mu_i}}}$	LOCATION
i	$(cm)^2$	$(deg)^2$		$(cm)^2$	$(deg)^2$		
0'	$(2.58)^2$	$(27.3)^2$	1.00	$(3.51)^2$	$(35.1)^2$	1.00	Upper center of hangar face
1	$(2.36)^2$	$(22.3)^2$	0.91	$(2.62)^2$	$(25.5)^2$	0.75	
2	$(2.36)^2$	$(22.3)^2$	0.91	$(2.62)^2$	$(25.5)^2$	0.75	
6	$(2.23)^2$	$(19.2)^2$	0.86	$(1.80)^2$	$(19.8)^2$	0.71	
7	$(2.23)^2$	$(19.2)^2$	0.86	$(1.80)^2$	$(19.8)^2$	0.71	
0	$(6.05)^2$	$(50.4)^2$	2.34	$(5.09)^2$	$(21.3)^2$	1.45	Center of pad
3'	$(4.20)^2$	$(33.5)^2$	1.63	$(3.11)^2$	$(20.6)^2$	0.89	
4'	$(4.20)^2$	$(33.5)^2$	1.63	$(3.11)^2$	$(20.6)^2$	0.89	

N.B. Only $(0.183\ cm)^2_{all\ i}$ $(2.1\ deg)^2_{i=0}$ of lateral variance and only $(0.377\ cm)^2_{all\ i}$ $(4.3\ deg)^2_{i=0}$ of vertical variance are caused by the combined variances in aircraft orientation angles (σ^2_ψ, σ^2_θ, σ^2_φ) from Table 6. Balances of variances in viewing angles are caused by variances in components of aircraft translation ($\sigma^2_{x_B}$, $\sigma^2_{y_B}$, $\sigma^2_{z_B}$) from Table 6.

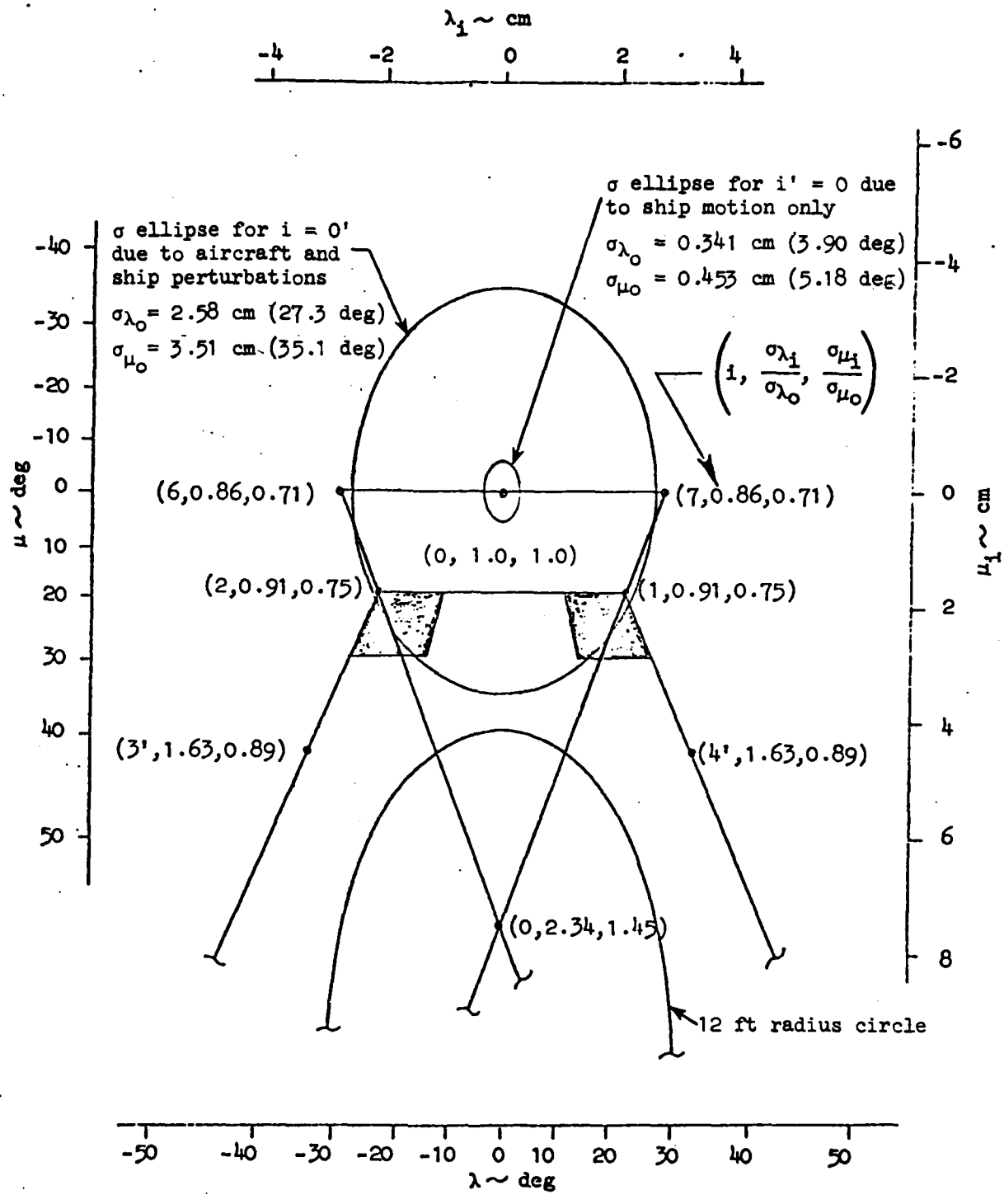

λ,μ = Viewing angle (this scale may be used to determine the subtended vertical or horizontal angle of any point on the pad)

Figure 23. Graphical Representation of σ Variation in Field of View for the R_m = 0 Case. (Viewing angles are preserved when page is held 5 cm in front of eye)

requirement to accommodate even one standard deviation of the boresight point in this extremely severe disturbance environment is apparent. Beside each of the points of regard in Figs. 22 and 23 we have shown a sequence of three numbers representing, in order from left to right, the numerical identification of the point i, the lateral coordinate variance ratio, $\sigma^{(cm)}_{\epsilon_{FOV_{\lambda_i}}} / \sigma^{(cm)}_{\epsilon_{FOV_{\lambda_o}}}$, and the vertical coordinate variance ratio, $\sigma^{(cm)}_{\epsilon_{FOV_{\mu_i}}} / \sigma^{(cm)}_{\epsilon_{FOV_{\mu_i}}}$. These extreme estimates of variability confirm the desirability, from the standpoint of reducing field-of-view requirements, of providing visual cues and visual aids above the hangar for assisting the pilot in arresting the approach and providing hovering guidance.

These extreme estimates of variability also emphasize the need for high authority, high bandwidth flight control systems in order to function effectively in this environment — much higher than is typical of current helicopter practice. The allowable aircraft motions due to all causes are only a few feet — Ref. 42 states "3 to 4 ft" in "allowable" touchdown error. If we interpret "allowable" as 2σ, Table 6 shows that the square root of the sum of the x- and y-variances in deck motion alone at the center of the pad slightly exceeds this "allowable" touchdown error. Without chasing the deck, this allowable touchdown error thus represents the best precision one might expect from a guidance and control system which regulates so well that no errors are contributed by aerodynamic disturbances or the pilot's divided attention. Graphic representation from the pilot's stationkeeping perspective of this apparent σ-variation in the center of the pad due to ship motion alone is shown by the smallest central σ-ellipse at 50 ft range-to-go in Fig. 22 and at zero range-to-go in Fig. 23.

With this assessment of the variability in the viewing angles required of the pilot with respect to his cockpit reference, we conclude our analyses of field of view requirements in the extremely severe disturbance environment to be expected in sea state 5 with 43 kt wind-over-deck. The predicted field of view requirements with manual control appear to be so great that more confidence is needed in the validity of the predicted airwake disturbance environment on which this analysis is predicated before these expectations can be converted into design requirements for field of view which are, in turn, based on high authority, high bandwidth flight control systems.

SECTION IV

SUMMARY AND CONCLUSIONS

A. SUMMARY

The field of view (FOV) from the aircraft cockpit required to see a point of regard on the recovery area during an approach to hovering over the area is a function of (a) the location of the point of regard itself on the ship, (b) the aircraft orientation, and (c) the relative position of the aircraft with respect to the ship, but the FOV may be restricted by cockpit occlusions.*

In Section III we have illustrated how the location of the point of regard on the ship and how the relative position of the undisturbed aircraft with respect to the ship affect the pilot's field of view from several types of approaching trajectories, which are described in Section II. The field-of-view requirements will be greatest near the ship in hovering and near-hovering flight above the recovery area. Tabular summaries of undisturbed aircraft field-of-view requirements for important points of regard are presented in this section following the conclusions. The selected points of regard are (a) the upper port corner of the hangar near the glide slope indicator (GSI), (b) the most forward line-up light on deck near the landing signal officer/mate, and (c) the center of the landing pad. Each tabular summary is for one particular point of regard and is arranged as a function of range-to-go and type of trajectory.

In addition to the undisturbed aircraft field-of-view requirements, we have illustrated in Section III how the effects of rotational and translational disturbances in the controlled aircraft motion combine to increase further the hovering and near-hovering field-of-view requirements. The

---

* Cockpit occlusions have been examined by Roberts (Ref. 2), Flynn (Ref. 4), Niemczyk (Ref. 5), and Jewell, et al (Ref. 41). A method for introducing cockpit occlusions into the field-of-view analysis is presented in Ref. 41.

details of the extensive analyses required to provide the examples presented here are documented in Refs. 33 and 41. The results depend in a critical way on the predicted model of the ship's airwake disturbance environment for sea state 5 and 43 kt wind-over-deck. The results take into account the combined variability in field of view caused by rolling, pitching, yawing, surging, swaying, and heaving degrees of freedom of the aircraft as the pilot attempts to guide and control the aircraft over the recovery area on the moving ship.

Two examples of perturbed field-of-view requirements are presented: (1) from 50 ft range-to-go (to the hovering point) on a constant relative bearing trajectory and (2) from the hovering point itself 40 ft above the center of the landing pad. For selected points of regard by the pilot we can estimate Gaussian statistical variances in the required field of view in cartesian picture plane coordinates caused by the predicted variances in the six aircraft degrees of freedom. Corresponding distributions of perturbations in terms of viewing angles will, however, tend to be increasingly skewed as the point of regard departs from the optical axis of the picture plane, because of the tangent relationship between picture plane coordinates and viewing angles. Nevertheless we can approximate the (non-Gaussian) angular variances in the field of view in terms of the (Gaussian) variances in the picture plane coordinates in order to provide a statistical measure of the additional field-of-view requirements imposed by the disturbance environment on the aircraft. The results of the variance estimation are identified by the symbol σ^2 below the corresponding nominal or average angular entries in the tables at the end of this section.

Table 9 shows that, in hovering at zero range-to-go, the vertical field of view required to observe (plus or minus) one standard deviation of the upper port corner of the hangar would be -34 ± 20 deg over the nose, assuming maximum sideslip and horizontal pitch attitude. The corresponding (plus or minus) standard deviation in the lateral field of view would be $\pm$ 19 deg. If instead, one were to assume no sideslip, the same vertical field requirement would apply, but the lateral requirement would become -28 ± 19 deg (negative left of the nose for an approach from the starboard quarter of the ship).

Table 10 shows that, in hovering at zero range-to-go, the vertical field of view required to observe (plus or minus) one standard deviation of the most forward line-up light would increase to -53 ± 25 deg, but the lateral requirement would become -22 ± 22 deg, assuming no sideslip.

Finally, Table 11 shows that, even with 50 ft of range still to go on the constant bearing trajectory, the vertical field of view required to observe (plus or minus) one standard deviation of the center of the landing pad would be -43 ± 24 deg, but the lateral requirement would become -20 ± 17 deg, assuming no sideslip.

These extreme estimates of variability confirm the desirability, from the standpoint of reducing field-of-view requirements, of providing visual cues and visual aids above the hangar for assisting the pilot in arresting the approach and providing hovering guidance.

These extreme estimates of variability also emphasize the need for high authority, high bandwidth flight control systems in order to function effectively in this environment — much higher than is typical of current helicopter practice. The allowable aircraft motions due to all causes are only a few feet — Ref. 42 states "3 to 4 ft" in "allowable" touchdown error. If we interpret "allowable" as 2σ, Table 6 shows that the square root of the sum of the x- and y-variances in deck motion alone at the center of the pad slightly exceeds this "allowable" touchdown error. Without chasing the deck, this allowable touchdown error thus represents the best precision one might expect from a guidance and control system which regulates so well that no errors are contributed by aerodynamic disturbances or the pilot's divided attention.

The predicted field of view requirements with manual control appear to be so great that more confidence is needed in the validity of the predicted airwake disturbance environment on which this study is predicated before these expectations are converted into design requirements for field of view which are, in turn, based on high authority, high bandwidth flight control systems. Validation of the airwake environment for V/STOL operations with non-aviation ships, therefore, is one recommendation resulting from this study. Subsequent validation of the reduced field of view requirements with high authority high bandwidth automatic flight control systems is another recommendation resulting from this study.

If airwake turbulence should prove to be as upsetting in reality as the present model suggests, the aircraft with its control system needs to achieve higher crossover frequencies in translational degrees of freedom. Depending on technique, this may also require higher crossover frequencies in roll and pitch axes. This may require a careful tradeoff of the roles of manual and automatic control in order to keep the pilot's intermittent/divided attention noise from compromising precision in stationkeeping.

B. CONCLUSIONS

The following conclusions about the nominal aircraft-to-ship field of view requirements in the absence of disturbances are based on the projections shown in Figs. 14 through 18 in Section III coupled with the trajectories described in Section II. Fold-out pages following this page provide a substantiating tabular summary of results organized to correspond with the conclusions. Each fold-out page may be examined simultaneously with the list of conclusions.

1. Homing trajectory (Fig. 14)

   a. Vertical field is smallest since angle over the nose is least until over the deck.

   b. Lateral field is smallest, if sideslip angle is zero.

---

2. Straight line trajectory (Fig. 15)

   a. Vertical field is larger, but ship may not disappear from view as early as in constant sink rate.

   b. Lateral field is greatest, if sideslip angle is zero.

---

3. Constant bearing trajectory (Fig. 16)

   a. Vertical field is restricted, since over-the-nose depression varies only between glide slope angle and zero until over deck.

   b. Lateral field is smallest, if aircraft heading is maintained constant.

---

4. Constant sink rate trajectory (Fig. 17)

   a. Vertical field is greatest — ship may disappear from view below nose at considerable range.

   b. Lateral field is same as for constant bearing.

---

5. Constant altitude trajectory (Fig. 18)

   a. Vertical field is approximately the same as for homing.

   b. Lateral field is same as for constant bearing.

TABLE 9

PILOT'S VERTICAL (a) AND LATERAL (b) LINE OF SIGHT ANGLES (DEG)
RELATIVE TO A HORIZONTAL AIRCRAFT CENTERLINE THROUGH FLIGHT EYE POSITION
REQUIRED TO OBSERVE UPPER PORT CORNER OF HANGAR (GLIDE SLOPE INDICATOR)
FOR VARIOUS TRAJECTORIES STARTING FROM 30 DEG OFF THE STARBOARD QUARTER OF A DD963

(All trajectories start with aircraft velocity 100 kt, decelerate at 0.1 g, and terminate with aircraft matching ship's velocity 20 kt)

	Slant Range to Nominal Hover Point Over Center of Pad at Height of Ship's Aft Stack					Remarks
	700 ft	400 ft	200 ft	50 ft	0	
1.						
a.	-5	-6	-7.5	-16	-34	(negative below horizon)
b.	-1	-2	-4	-14	-28	(negative left of nose and assuming no side slip)
2.						
a.	-9.5	-12	-16	-29	-34	
b.	-21	-26	-34	-44	-28	(assuming no sideslip)
3.						for sea state 5 with 43 kt wind-over-deck, approximate variance is denoted by σ^2 (deg)^2
a.	-8	-9	-11	-18 $\sigma^2 = (19)^2$	-34 $\sigma^2 = (20)^2$	
b.	-10	-12	-15	-20 $\sigma^2 = (10)^2$	-28 $\sigma^2 = (19)^2$	(assuming no sideslip)
	0	0	0	0	0	(assuming max sideslip)
4.						
a.	-14	-19	-26	-42	-34	
b.						
5.						
a.	-2	-3.3	-5.7	-15	-34	
b.						

TABLE 10

PILOT'S VERTICAL (a) AND LATERAL (b) LINE OF SIGHT ANGLES (DEG)
RELATIVE TO A HORIZONTAL AIRCRAFT CENTERLINE THROUGH FLIGHT EYE POSITION
REQUIRED TO OBSERVE MOST FORWARD LINE-UP LIGHT ON DECK
FOR VARIOUS TRAJECTORIES STARTING FROM 30 DEG OFF THE STARBOARD QUARTER OF A DD963

(All trajectories start with aircraft velocity 100 kt, decelerate at 0.1 g, and terminate with aircraft matching ship's velocity 20 kt)

	Slant Range to Nominal Hover Point Over Center of Pad at Height of Ship's Aft Stack					Remarks
	700 ft	400 ft	200 ft	50 ft	0	
1.						
a.	-7	-8	-12	-29	-53	(negative below horizon)
b.	+2 (Right) -1 (Left)	+4 (Right) -2 (Left)	+6 (Right) -4 (Left)	±12 (R/L)	±22 (R/L)	(negative left of nose and assuming no sideslip)
2.						
a.	-11	-14	-20	-40	-53	
b.	-21	-26	-34	-47	±22 (R/L)	(assuming no sideslip)
3.						for sea state 5 with 43 kt wind-over-deck, approximate variance is denoted by σ^2 (deg)^2
a.	-9	-11	-15	-30 $\sigma^2 = (20)^2$	-53 $\sigma^2 = (25)^2$	
b.	-10	-12	-15	-20 $\sigma^2 = (11)^2$	-22 $\sigma^2 = (22)^2$	(assuming no sideslip)
	0	0	0	0	0	(assuming max sideslip)
4.						
a.	-15	-21	-30	-52	-53	
b.						
5.						
a.	-3.1	-5.5	-10	-27	-53	
b.						

TABLE 11

PILOT'S VERTICAL (a) AND LATERAL (b) LINE OF SIGHT ANGLES (DEG)
RELATIVE TO A HORIZONTAL AIRCRAFT CENTERLINE THROUGH FLIGHT EYE POSITION
REQUIRED TO OBSERVE CENTER OF LANDING PAD
FOR VARIOUS TRAJECTORIES STARTING FROM 30 DEG OFF THE STARBOARD QUARTER OF A DD963

(All trajectories start with aircraft velocity 100 kt, decelerate at 0.1 g, and terminate with aircraft matching ship's velocity 20 kt)

	Slant Range to Nominal Hover Point Over Center of Pad at Height of Ship's Aft Stack					Remarks
	700 ft	400 ft	200 ft	50 ft	0	
1.						
a.	-7	-8.3	-13	-39	-90	(negative below horizon)
b.	0	0	0	0	(→ 0)	(assuming no sideslip)
2.						
a.	-12	-15	-23	-51	-90	
b.	-21	-27	-37	-64	(→ -90)	(negative left of nose and assuming no sideslip)
3.						for sea state 5 with 43 kt wind-over-deck, approximate variance is denoted by σ^2 (deg)^2
a.	-9.2	-12	-17	-43 $\sigma^2 = (24)^2$	-90 $\sigma^2 = (21)^2$	
b.	-10	-12	-15	-20 $\sigma^2 = (17)^2$	(→ -30) $\sigma^2 = (50)^2$	(assuming no sideslip)
	0	0	0	0	(→ 0)	(assuming max sideslip)
4.						
a.	-16	-22	-34	-68	-90	
b.						
5.						
a.	-3.3	-5.7	-12	-39	-90	
b.						

REFERENCES

1. Ringland, Robert F., Samuel J. Craig, and Warren F. Clement, Survey of Piloting Factors in Fixed-Wing V/STOL Aircraft Design, Systems Technology, Inc., Technical Report 1082-1, Nov. 1976.

2. Roberts, Edward O., External Visibility Criteria for VTOL Aircraft, AFFDL-TR-67-27, Mar. 1967.

3. Thielges, J. R., and W. G. Matheny, "A Review of the Analysis of Visual Discriminations in Helicopter Control," HumRRO Paper 4-66, Apr. 1966.

4. Flynn, Cdr. Noel S., USN, Requirements for VLA Systems, Navy-NASA V/STOL Flying Qualities Workshop, Naval Postgraduate School Monterey, CA, 26-28 Apr. 1977, pp. 477-494.

5. Niemczyk, R., and T. Momiyama, "NAVTOLAND (Navy VTOL Capability Development)," SAE Aerospace Control and Guidance Systems Committee Meeting No. 41, Palo Alto, CA, 1-3 March 1978.

6. Gibson, J. J., The Perception of the Visual World, Boston, Houghton Mifflin, 1950, Chaps. 6-7.

7. Graham, C. H., "Visual Perception," In A Handbook of Experimental Psychology (Ed., S. S. Stevens), John Wiley, New York, 1951, pp. 868-920.

8. Gilinsky, A. S., "Perceived Size and Distance in Visual Space," Psychol. Rev., Vol. 58, 1951, pp. 460-482.

9. Gilinsky, A. S., "The Effect of Attitude Upon the Perception of Size," Am. J. Psych., Vol. 68, No. 2, 1955, pp. 173-192.

10. Gordon, D. A., "Static and Dynamic Visual Fields in Human Space Perception," J. Opt. Soc. Amer., Vol. 55, No. 10, Oct. 1965, pp. 1296-1303.

11. Gordon, D. A., "Perceptual Basis of Vehicular Guidance," Public Roads, Vol. 34 (1966), pp. 53-68.

12. Calvert, E. S., "The Theory of Visual Judgments in Motion and Its Application to the Design of Landing Aids for Aircraft," London, Trans. Illum. Eng. Soc., Vol. 22, No. 10, 1957.

13. Havron, M. Dean, Information Available from Natural Cues During Final Approach and Landing, Human Sciences Research, Inc., Report HSR-RR-62/3-MK-X, Mar. 1962.

14. Naish, J. M., "Control Information in Visual Flight," Proc. 7th Annual Conference on Manual Control, NASA SP-281, June 1971 (also McDonnell Douglas Paper No. 5921).

15. Grunwald, A. J., and S. J. Merhav, "Vehicular Control by Visual Field Cues," IEEE Trans., Vol. SMC-6, No. 12, Dec. 1976, pp. 835-845.

16. McRuer, D. T., and E. S. Krendel, Mathematical Models of Human Pilot Behavior, AGARD-AG-188, Jan. 1974.

17. Noton, D., "A Theory of Visual Pattern Perception," IEEE Trans., Vol. SSC-6, No. 4, Oct. 1970, pp. 349-357.

18. Sanders, A. F., "Some Aspects of the Selective Process in the Functional Visual Field," Ergonomics, Vol. 13, No. 1, 1970, pp. 101-117.

19. Fitts, P. M., R. E. Jones, and J. L. Milton, "Eye Movements of Aircraft Pilots During Instrument-Landing Approaches," Aeronautical Engineering Review, Vol. 9, No. 2, Feb. 1950, pp. 24-29.

20. Weir, D. H., and R. H. Klein, The Measurement and Analysis of Pilot Scanning and Control Behavior During Simulated Instrument Approaches, NASA CR-1535, June 1970.

21. Young, R., L. Stark, and C. Kupfer, Physiology of the Visual Control System, NASA CR-238, June 1965.

22. Tierney, G. P., "VTOL Night Approach," Approach, Mar. 1967, pp. 28-29.

23. Lineback, H., R. Parkinson, and A. B. Hill, Shipboard Evaluation of Visual Landing Aid Systems for Non-Aviation Ships, NATC-FT-81R-71, 28 Oct. 1971.

24. Pinegar, Lt. F. A., USN, and H. G. Kolwey, HH-3F Helicopter/USCGC Hamilton (WHEC-715) Dynamic Interface Evaluation, NATC-RW-26R-76, 20 May 1976.

25. Middleton, W. E. Knowles, "Vision Through the Atmosphere," Canada: University of Toronto, 1952.

26. Frenk, R. S., D. E. Skaar, and J. A. Tennant, "Driver's Visual Detection," SAE Paper 720142 presented at the SAE Automotive Engineering Congress, Detroit, Michigan, 10-14 Jan. 1972.

27. Allen, R. W., and D. T. McRuer, "The Effect of Adverse Visibility on Driver Steering Performance in an Automobile Simulator," SAE Paper 770239, Mar. 1977.

28. Davies, E. B., Contrast Thresholds for Air to Ground Vision, RAE Technical Report 65089, Apr. 1965.

29. Blackwell, H. R., "Contrast Thresholds of the Human Eye," J. of the Optical Society of America, No. 36, 1946, pp. 624-643.

30. Blackwell, H. R., and D. W. McCready, Jr., "Foveal Detection Thresholds for Various Durations of Target Presentation," Minutes and Proceedings of NAS-NRC Vision Committee, Nov. 1952, ACSIL/53/4405.

31. Clement, Warren F., and Robert K. Heffley, Some Effects of Adverse Visibility on Threshold Properties of the Pilot's Perception in VTOL Approaches to Non-Aviation Ships, Systems Technology, Inc., Working Paper 1115-3, May 1978.

32. Heffley, Robert K., and Warren F. Clement, Development of General Closed Loop Pilot Vehicle Dynamics for VTOL Aircraft at Low Speeds, Systems Technology, Inc., Working Paper 1115-1, Apr. 1978.

33. Heffley, Robert K., Calculation of Total Motion Error Variance for Hovering Field of View Analyses, Systems Technology, Inc., Working Paper 1115-5, July 1978.

34. Heffley, Robert K., Computation and Analysis of V/STOL Approach Trajectories, Systems Technology, Inc., Working Paper 1122-1, March 1978.

35. Gordon, Donald A., "Experimental Isolation of Drivers' Visual Input," Public Roads, Vol. 33, No. 12, Feb. 1966, pp. 266-273.

36. Weir, David H., and Duane T. McRuer, Conceptualization of Overtaking and Passing on Two-Lane Rural Roads, Franklin Institute Research Laboratory, Technical Report No. 1-193, Dec. 1967.

37. Benedetto, R. A., Non-Aviation Ships Helicopter Facility Resume, NAEC ENG-7575, Rev. C, 1973.

38. Jane, Fred T., (Capt. John E. Moore, Ed.), Jane's Fighting Ships, McGraw Hill Book Co., N.Y., 1973-74, p. 420.

39. Alex, Fredric R., Geometric Foundation of Motion Perspective, Systems Technology, Inc., Working Paper 170-3, Jan. 1967.

40. Jewell, Wayne F., and Warren F. Clement, Computation of the Pilot's View of a Non-Aviation Ship's VTOL Pad for Several Types of Approach Trajectories, Systems Technology, Inc., Working Paper 1115-2, March 1978.

41. Jewell, Wayne F., and Warren F. Clement, Perturbations of the Pilot's View of a Non-Aviation Ship's VTOL Pad Due to Linear and Angular Perturbations of the Aircraft, Systems Technology, Inc., Working Paper 1115-4, Aug. 1978.

APPENDIX A

KINEMATICS FOR THE PERCEPTION OF TIME-ADVANCED LATERAL DEVIATION

γ = Nominal Glide Slope Angle

ν = Approach Line Up Centerline Perspective Angle

y = Lateral Displacement

h = Altitude

$\overline{F_1F_2}$ = Line Up Centerline

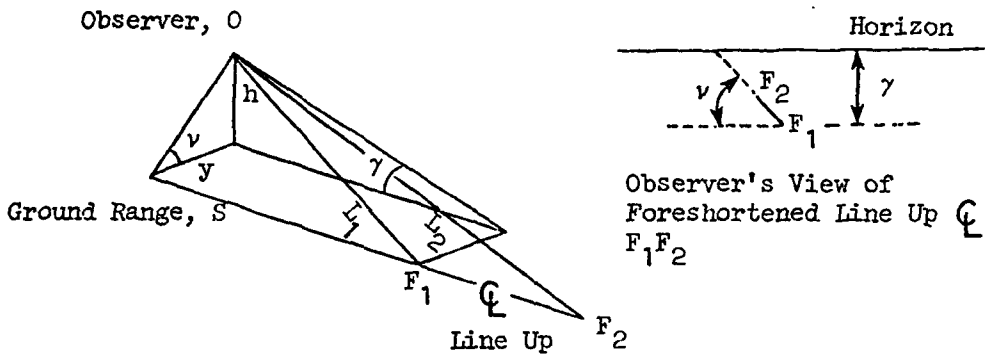

Figure A-1. Geometry for Perception of Time-Advanced Lateral Deviation

The ground range from the observer to the point of regard F_1 will be approximately S, if $y/S << 1$. Then

$$S \doteq V_G T_G + \frac{1}{2} a_x T_G^2$$

where V_G is ground speed, a_x is horizontal acceleration (negative for deceleration), T_G is time to go to the point of regard, and $\dot{y}/V_G << 1$; $\dot{y} = dy/dt$.

$$T_G = \begin{cases} -\frac{V_G}{a_x} \pm \sqrt{\left(\frac{V_G}{a_x}\right)^2 + \frac{2S}{a_x}} & \text{if } a_x < 0 \\ \frac{S}{V_G} & \text{if } a_x = 0 \end{cases}$$

But

$$y = h \cot \nu$$

$$\dot{y} = \dot{h} \cot \nu - h \csc^2 \nu \, \dot{\nu}$$

Since $\nu = 0(\frac{\pi}{2})$, $\cot \nu << \csc^2 \nu \doteq 1$ and since $\dot{h}/h << 1$, $\dot{y}/h \doteq -\dot{\nu}$

Therefore, by perceiving $\dot{\nu}$, the pilot perceives $\dot{y}/h$ approximately and associates this apparent lateral velocity with the point of regard F_1, which is advanced by distance S and time T_G in the future. The future lateral displacement at F_1 corresponding to constant $\dot{y}$ will be

$$y(t + T_G) \doteq y(t) + \dot{y}T_G \doteq h(\cot \nu - \dot{\nu}T_G) \doteq h(\tfrac{\pi}{2} - \nu - \dot{\nu}T_G)$$

The Laplace transform of $y(t + T_G)$ will be

$$\mathcal{L}[y(t + T_G)] = e^{T_G s} y(s) \doteq h(1 + T_G s)[(co\nu)(s)]$$

where $co\nu = (\frac{\pi}{2} - \nu)$ is usually small and s is the complex Laplacian operator. This is the basis for the equivalence between time-advanced lateral deviation and the simple lead, $(1 + T_G s)$, operating on the perceived complement of perspective angle, ν. The time T_G is like a time-varying derivative weighting coefficient through which the pilot can provide phase lead to the extent of perceived distance S, ground speed V_G, and acceleration a_x. Object size will provide distance cues and motion streamers will provide ground speed cues, perception of both of which may be limited by weather condition. Vestibular cues will provide a measure of deceleration, although it remains to be shown whether the pilot will lend much weight to the vestibular cues in this case.

APPENDIX B

COMPARISON OF POLAR AND CARTESIAN PICTURE PLANES

The two most common planar candidates for analyzing and describing visual field images are the polar "picture plane" and the cartesian picture plane.

POLAR PICTURE PLANE

The polar picture plane is somewhat misleading because it is actually a distorted planar representation of two spherical coordinates. It is applied to two V/STOL trajectories in Ref. B-1 and to the representation of human perceptual data in Ref. B-2. Besides the latter advantage, the polar picture plane easily includes the zenith, nadir, and temporal extremities of peripheral vision, which otherwise would require a cartesian plane of infinite extent in front of the eye and normal to a line of sight. The nadir and temporal extremities are expected to be important in hovering flight.

One can, in theory, map the images perceived by the eye on a spherical surface of arbitrary diameter centered at, for example, the pupil of either eye. Such a mapping would be in strict accordance with the principles of spherical trigonometry and would not therefore be rectifiable on a plane. Congruent visual representations on the page of a report would not be possible. Representation of motion perspective streamer vectors, defined by angular coordinates, on a polar picture plane calibrated linearly in degrees produces incongruent streamer images. This type of transformation does not offer attractive aspects for the analytical approach required for this investigation, although, as noted before, it is compatible with the representation of extensive human perceptual data in Ref. B-2.

CARTESIAN PICTURE PLANE

The trigonometry in a cartesian picture plane at an arbitrary distance from the eye and normal to a reference line of sight is much simpler, and the coordinates can be directly represented on the page of a report without distortion (e.g., straight ground lines appear straight). Kinematic transformations of motion perspective in the cartesian picture plane are applied to some typical airplane motions in Ref. B-3, which endorses the analytical advantages. Disadvantages recognized in Ref. B-3 include (1) the requirement for a very large picture plane close to the eye for representing visual angles approaching 90 deg off the reference line of sight and (2) varying requirements for the preferred orientation of the reference line of sight, depending on the specific flight profile, particularly in the case of V/STOL transition to a ship at sea. Another disadvantage is the need to apply an additional transformation to render motion perspective in the cartesian picture plane compatible with the representation of human perceptual data in Ref. B-2. We believe that these three disadvantages are over-balanced by the relative analytical advantage of the plane trigonometry in the cartesian picture plane.

REFERENCES

B-1 Roberts, Edward O., External Visibility Criteria for VTOL Aircraft, AFFDL-TR-67-27, Mar. 1967.

B-2 Haines, R. F., "A Review of Peripheral Vision Capabilities for Display Layout Designers," Proc. Soc. Inform. Display, Vol. 16, No. 4, 1975, pp. 238-249.

B-3 Alex, F. R., Geometric Foundation of Motion Perspective, Systems Technology, Inc., Working Paper No. 170-3, Jan. 1967.

END

DATE
FILMED

5 -83

DTIC